Supplementary Material for "Topological phonon blockade and its transfer via dark-mode engineering"

Deng-Gao Lai,[1,*] Adam Miranowicz,[1,2] and Franco Nori[1,3,4]

[1]*Theoretical Quantum Physics Laboratory, Cluster for Pioneering Research, RIKEN Wako-shi, Saitama 351-0198, Japan*
[2]*Institute of Spintronics and Quantum Information, Faculty of Physics and Astronomy, Adam Mickiewicz University, 61-614 Poznań, Poland*
[3]*RIKEN Center for Quantum Computing (RQC), 2-1 Hirosawa, RIKEN Wako-shi, Saitama 351-0198, Japan*
[4]*Physics Department, University of Michigan, Ann Arbor, Michigan 48109-1040, USA*

In this Supplementary Material, we show detailed results on topological phonon transfer and topological phonon blockade enabled via dark-mode engineering which is induced by synthetic magnetism, in phase-dependent loop-coupled optomechanical configurations. Specifically, this document consists of five sections on: (i) Physical system and its dark-mode engineering; (ii) Effective non-Hermitian Hamiltonian and its exceptional point; (iii) Dark-mode-engineered topological phononics; (iv) Scalable network-based topological phonon transfer enabled by synthetic magnetism; and (v) Quantum collective motion using dark-mode engineering.

Contents

I. Physical system and dark-mode engineering 2
A. Physical model and its Hamiltonian 2
B. Dark and bright modes 3
C. Dark-mode engineering 5

II. Effective non-Hermitian Hamiltonian and its exceptional point 7
A. Effective non-Hermitian Hamiltonian 7
B. Exceptional point 10
C. Malfunction and function of the exceptional point 12
D. Inactivation and activation of topological operations 13
E. Eigenvalue distributions around an exceptional point 14

III. Dark-mode-engineered topological phononics 14
A. Efficiency of topological phonon transfer 14
B. Topological phonon blockade and its transfer by engineering dark modes 15
C. Dark-mode-engineered nonreciprocal topological dynamics 16

IV. Scalable network-based topological phonon transfer via synthetic magnetism 16
A. Dark-mode engineering in quantum optomechanical networks 17
B. Scalable network-based topological phonon transfer 20

V. Quantum collective motion using dark-mode engineering 20
A. Dark–bright mode engineering 20
B. Occupations of dark and bright modes 21
C. Quantum collective ground-state preparation of both dark and bright modes 21

References 22

*Electronic address: denggaolai@foxmail.com

I. PHYSICAL SYSTEM AND DARK-MODE ENGINEERING

Nonreciprocal topology is engendered by imposing topological operations winding around an exceptional point (EP), and it extremely fragile in face of all dark modes. As a result, these dark modes enable the deactivation of topological operations and EPs, which leads to a complete blockade of both mode conversion and phonon transfer between dark and bright modes. In this work, we show how to overcome this outstanding challenge and to achieve a versatile yet unique nonreciprocal topological phonon transfer (TPT) and topological phonon blockade (TPB) via dark-mode engineering. This is achieved by employing synthetic magnetism, which results in a flexible transition between the dark-mode-nonbreaking ($\mathcal{DMN}$) and dark-mode-breaking ($\mathcal{DMB}$) regimes, in a precise and controlled manner. For example, we find that when the system operates in the $\mathcal{DMN}$ regime, TPB happens; while TPT is observed in the $\mathcal{DMB}$ regime, which offers an exciting opportunity of bridging TPB and TPT at will, having no counterpart in all previous studies. In particular, we apply the dark-mode-engineering mechanism to quantum networks, making the dark-mode-immune network-based TPT from dark to bright modes feasible. Our study maps a general path towards generating profoundly different nonreciprocal topological quantum resources with immunity against dark modes. In a broader view, our study sheds new light on the combination of dark-mode engineering, topological operations, and quantum networks, and offers an exciting prospect of revealing a unique topology with immunity against dark modes.

In this section, the quantum Langevin equations for both photon and phonon modes are detailedly derived in a loop-coupled three-mode optomechanical system, where a common photon mode optomechanically coupled to two phonon modes, which are coupled to each other via a phase-dependent phonon-hopping interaction. Then, the linearized optomechanical Hamiltonian of our system can be derived by applying the linearization procedure and then, we study in detail the dark mode and the dark-mode engineering, which is enabled by the synthetic magnetism.

A. Physical model and its Hamiltonian

In this section, we focus on quantum optomechanical networks, which consist of N phonon modes coupled to a common photon mode through radiation-pressure couplings. The nearest-neighboring phonon modes are coupled to each other via phase-dependent phonon-hopping interactions. Then, the Hamiltonian of quantum optomechanical networks reads ($\hbar = 1$)

$$\mathcal{H} = \omega_c a^\dagger a + \sum_{j=1}^{N}[\omega_j b_j^\dagger b_j + g_j a^\dagger a(b_j^\dagger + b_j)] + \sum_{j=1}^{N-1}\xi_j(e^{i\Theta_j} b_j^\dagger b_{j+1} + e^{-i\Theta_j} b_{j+1}^\dagger b_j) + i\sqrt{\kappa_{\rm in}}\epsilon_{\rm in}(a^\dagger e^{-i\omega_l t} - \text{H.c.}), \tag{S1}$$

where the operators $a^\dagger$ (a) and $b_j^\dagger$ (b_j) are creation (annihilation) operators of the photon mode and the jth phonon mode, with resonance frequencies ω_c and ω_j, respectively. The g_j terms denote the optomechanical interactions between the photon mode and the jth phonon mode, with the parameter g_j being the single-photon optomechanical-coupling strength. The laser driving of the system is described by the $\epsilon_{\rm in} = \sqrt{P/(\hbar\omega_L)}$ term, with the laser power P, frequency ω_L, linewidth κ, and input-coupling rate $\kappa_{\rm in}$. In addition, we introduce the phase-dependent phonon-hopping interactions between the nearest-neighboring phonon modes, with the coupling strengths ξ_j and modulation phases Θ_j. A synthetic gauge field, which is employed for engineering all dark modes, can be induced on demand, using phase-dependent loop-coupled setups, made up of the g_j and ξ_j terms.

To facilitate a clear understanding of the proposed dark-mode engineering and its underlying physical mechanisms, we first consider the simplest three-mode optomechanical devices (i.e., $N = 2$) consisting of two phonon modes coupled to a shared photon mode. In this case, we study in detail both TPT and TPB between the dark and bright modes, and it is achieved by employing dark-mode engineering. Specifically, a unique photon mode is supported by an optomechanical cavity with an external laser driving, leading to the in-parallel optomechanical couplings of the photon mode to the two phonon modes via radiation-pressure radiation, and the two phonon modes are coupled to each other via a phase-dependent phonon-exchange interaction. Note that a related three-mode optomechanical system has recently been reported in experiments and proposals, and especially, it has already been implemented using state-of-the-art technology to achieve topological responses, *fully evading* dark modes [S1, S2]. Consequently, the Hamiltonian of the two-phonon-mode optomechanical system reads

$$\mathcal{H} = \omega_c a^\dagger a + \sum_{j=1,2}[\omega_j b_j^\dagger b_j + g_j a^\dagger a(b_j^\dagger + b_j)] + \xi(e^{i\Theta} b_1^\dagger b_2 + e^{-i\Theta} b_2^\dagger b_1) + i\sqrt{\kappa_{\rm in}}\epsilon_{\rm in}(a^\dagger e^{-i\omega_l t} - \text{H.c.}), \tag{S2}$$

where a synthetic gauge field, which is employed to flexibly manipulate the dark mode, can be induced on demand by the ξ term, with a modulation phase Θ and a phonon-exchange coupling strength ξ between the two phonon modes.

For a standard optomechanical system which is composed of a photon mode linearly coupled to a single phonon mode, a pair of coupled differential equations for both photon and phonon modes are resulted from an input–output approach to these systems. Subsequently, these equations of motion can be easily treated in the Fourier domain for better understanding the optical modification of the mechanical susceptibilities. Here, we concentrate on a simple extension of these standard models, by

considering two phonon modes, each of which is coupled to a common photon mode. Subsequently, this leads to the following equations of motion for both photon and phonon modes, i.e.,

$$\dot{a} = -\left(\frac{\kappa}{2} + i\omega_c\right)a - ig_1 a z_1 - ig_2 a z_2 + \sqrt{\kappa_{\rm in}}\epsilon_{\rm in}, \tag{S3a}$$

$$\dot{b}_1 = -\left(\frac{\gamma_1}{2} + i\omega_1\right)b_1 - ig_1 a^\dagger a - i\xi e^{i\Theta}b_2 + \sqrt{\gamma_1}\eta_1, \tag{S3b}$$

$$\dot{b}_2 = -\left(\frac{\gamma_2}{2} + i\omega_2\right)b_2 - ig_2 a^\dagger a - i\xi e^{-i\Theta}b_1 + \sqrt{\gamma_2}\eta_2, \tag{S3c}$$

where the parameters κ and $\kappa_{\rm in}$ are the dissipation rate of the linewidth and the input coupling rate of the cavity field, respectively; $z_j = b_j^\dagger + b_j$ is the position operator for the jth phonon mode. In addition, ω_j, g_j, and γ_j are the mechanical resonance frequency of the jth phonon mode, the single-photon coupling strength of the photon mode and the jth phonon mode, and the mechanical dissipation rate of the jth phonon mode, respectively. The optical and vibrational modes are driven by the input fields $\epsilon_{\rm in}$ and η_j, respectively.

Then, a linearization procedure can be applied so that one can simplify the physical model by considering the case in the strong-driving regime of quantum systems. Specifically, both photon and phonon operators used in Eq. (S3) can be expressed as sums of their classical averages and quantum fluctuations, i.e.,

$$a = \bar{a} + \delta a, \quad b_j = \bar{b}_j + \delta b_j. \tag{S4}$$

By separating the classical motion from their quantum fluctuations, the equations of motion for the classical-motion variables can be obtained and then, we have the classical average of the optical dynamical variable:

$$\bar{a} = \frac{\sqrt{\kappa_{\rm in}}\epsilon_{\rm in}}{\kappa/2 - i\Delta}, \tag{S5}$$

where the parameter $\Delta \approx \omega_L - \omega_c$ is the driving detuning. Subsequently, we can easily obtain the linearized equations of motion for quantum fluctuations, defined as:

$$\delta\dot{a} = -\left(\frac{\kappa}{2} - i\Delta\right)\delta a - iG_1\delta z_1 - iG_2\delta z_2, \tag{S6a}$$

$$\delta\dot{b}_1 = -\left(\frac{\gamma_1}{2} + i\omega_1\right)\delta b_1 - i\left(G_1^*\delta a + G_1\delta a^\dagger\right) - i\xi e^{i\Theta}\delta b_2 + \sqrt{\gamma_1}\eta_1, \tag{S6b}$$

$$\delta\dot{b}_2 = -\left(\frac{\gamma_2}{2} + i\omega_2\right)\delta b_2 - i\left(G_2^*\delta a + G_2\delta a^\dagger\right) - i\xi e^{-i\Theta}\delta b_1 + \sqrt{\gamma_2}\eta_2, \tag{S6c}$$

where the parameter $G_{j=1,2} = g_j\bar{a}$ is the linearized optomechanical-coupling strength between the photon mode and the jth phonon mode.

Below, the dark and bright modes are studied in detail in the three-mode optomechanical systems, which consists of two phonon modes coupled to a common photon mode. In addition, the dark mode and its breaking in this system is analyzed in detail. We see in Eq. (S6) that these photon and phonon modes are coupled to each other via the bilinear-form interactions. Mathematically, an effective Hamiltonian can be easily inferred to govern these bilinear interactions, including both beam-splitting-type (excitation-exchanging) terms and the two-mode-squeezing (excitation-creating) terms.

In our studied optomechanical TPT, the linearized couplings in this system are dominated by the beam-splitting-type interactions of these bosonic modes and therefore, the system Hamiltonian can be easily simplified by assuming the rotating-wave approximation (RWA). As a result, the linearized Hamiltonian takes the following form discarding the noise terms:

$$\mathcal{H}_{\rm lin} = -\Delta\delta a^\dagger\delta a + \sum_{j=1}^{2}[\omega_j\delta b_j^\dagger\delta b_j + G_j(\delta a\delta b_j^\dagger + \delta b_j\delta a^\dagger)] + \xi(e^{i\Theta}\delta b_1^\dagger\delta b_2 + e^{-i\Theta}\delta b_2^\dagger\delta b_1), \tag{S7}$$

where the parameter $\Delta \approx \omega_L - \omega_c$ is the driving detuning. Below, we analyze in detail both the dark and bright modes based on the Hamiltonian $\mathcal{H}_{\rm lin}$ in Eq. (S7).

B. Dark and bright modes

As is well known, topological phenomena in topological physics are generally destroyed by dark modes naturally decoupled from the system, which results in a complete deactivation of both EPs and topological operations. For example, TPT and mode switching can always happen when executing adiabatic closed paths enclosing an EP. Surprisingly, once dark modes are

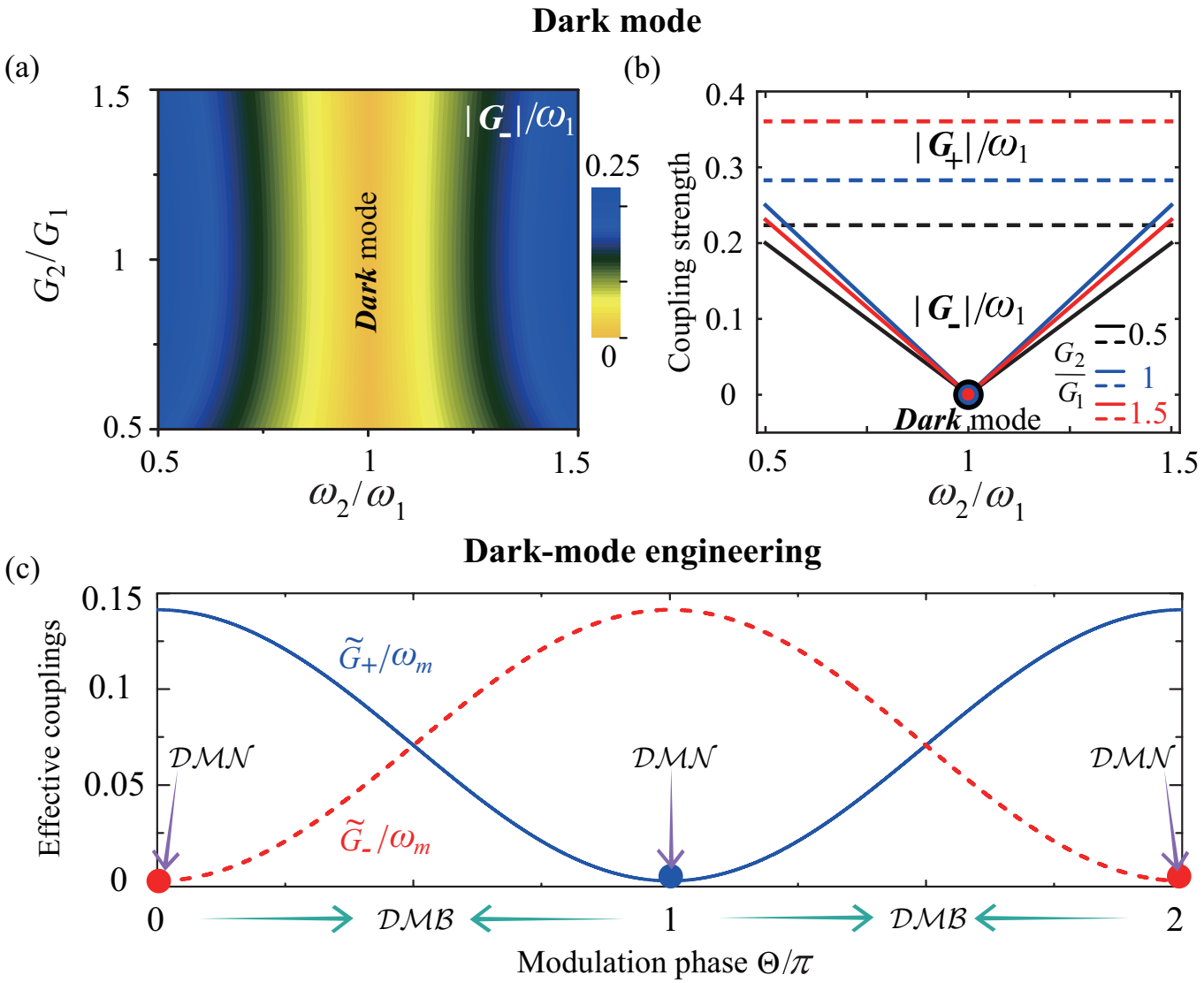

FIG. S1: (a) Coupling strength $|G_-|/\omega_1$ versus the frequency ratio ω_2/ω_1 and the optomechanical-coupling-strength ratio G_2/G_1 of the two phonon modes. (b) Coupling strengths $|G_+|/\omega_1$ (dashed lines) and $|G_-|/\omega_1$ (solid lines) versus the frequency ratio ω_2/ω_1 when G_2/G_1=0.5 (black lines), 1 (blue lines), and 1.5 (red lines). Here we set $G_1/\omega_1 = 0.2$. (c) Redefined coupling strengths $\tilde{G}_+/\omega_m$ and $\tilde{G}_-/\omega_m$ versus the modulation phase Θ. Here we set the resonance frequency ω_m as the frequency scale, and assume $G_j/\omega_m = \xi/\omega_m = 0.1$ and $\omega_j/\omega_m = 1$.

possessed by the system, both the mode conversion and TPT between dark and bright modes are unfeasible regardless of the adjustment of adiabatic trajectories and system parameters, due to the dark-mode-induced destruction of topological operations and EPs.

In this section, we study in detail both the dark and bright modes in our three-mode optomechanical system, by demonstrating the cases where the synthetic magnetism is absent (i.e., $\xi = 0$) and present (i.e., $\xi \neq 0$ and $\Theta \neq n\pi$), respectively.

Specifically, in the absence (i.e., $\xi = 0$) of the synthetic magnetism induced by the phase-dependent loop-coupled configurations, the system Hamiltonian (S7) becomes

$$\mathcal{H}_{\rm lin} = -\Delta\delta a^\dagger \delta a + \sum_{j=1}^{2}[\omega_j \delta b_j^\dagger \delta b_j + G_j(\delta a \delta b_j^\dagger + \delta b_j \delta a^\dagger)]. \tag{S8}$$

In this system, the two phonon modes δb_1 and δb_2, which are coupled to a common photon mode δa, form the following two

motional normal modes:

$$\mathcal{B}_+ = \frac{G_1\delta b_1 + G_2\delta b_2}{\sqrt{G_1^2+G_2^2}}, \quad \textit{bright} \text{ mode}, \tag{S9}$$

$$\mathcal{B}_- = \frac{G_2\delta b_1 - G_1\delta b_2}{\sqrt{G_1^2+G_2^2}}, \quad \textit{dark} \text{ mode}. \tag{S10}$$

Note that the bosonic commutative relations (i.e., $[\mathcal{B}_\pm, \mathcal{B}_\pm^\dagger] = 1$) are satisfied by the above vibrational normal modes $\mathcal{B}_\pm$. The system Hamiltonian in Eq. (S8) can be rewritten with these two vibrational normal modes $\mathcal{B}_\pm$ as

$$\mathcal{H}_{\rm lin} = -\Delta\delta a^\dagger\delta a + \omega_+\mathcal{B}_+^\dagger\mathcal{B}_+ + \omega_-\mathcal{B}_-^\dagger\mathcal{B}_- + G_+(\delta a\mathcal{B}_+^\dagger + \mathcal{B}_+\delta a^\dagger) + G_-(\mathcal{B}_+^\dagger\mathcal{B}_- + \mathcal{B}_-^\dagger\mathcal{B}_+), \tag{S11}$$

where $\omega_\pm$ and $G_\pm$ are the resonance frequencies and the coupling strengths, respectively, defined as:

$$\omega_+ = \frac{G_1^2\omega_1 + G_2^2\omega_2}{G_1^2+G_2^2}, \quad \omega_- = \frac{G_2^2\omega_1 + G_1^2\omega_2}{G_1^2+G_2^2}, \tag{S12a}$$

$$G_+ = \sqrt{G_1^2+G_2^2}, \qquad G_- = \frac{G_1G_2(\omega_1-\omega_2)}{G_1^2+G_2^2}. \tag{S12b}$$

In the absence of the synthetic magnetism (i.e., $\xi = 0$), it is seen from in Eqs. (S11) and (S12b) that when $\omega_1 = \omega_2$, the normal mode $\mathcal{B}_-$ is completely decoupled (i.e., $G_- = 0$) from the system, indicating the emergence of a dark mode (i.e., $\mathcal{B}_-$). In stark contrast to this, the normal mode $\mathcal{B}_+$ is a bright mode because of an effective coupling (i.e., $G_+ > 0$) of $\mathcal{B}_+$ to the system. The dark mode is decoupled from the system, resulting in a complete blockade of both mode conversion and phonon transfer between the dark and bright modes.

To further elucidate this point, we display in Fig. S1(a) the redefined light-motion coupling strength $|G_-|/\omega_1$ versus the coupling-strength ratio (i.e., G_2/G_1) and the resonance frequency ratio (i.e., ω_2/ω_1) of the two phonon modes. Clearly, it reveals that without the synthetic magnetism (i.e., $\xi = 0$) and $\omega_2 = \omega_1$, we counterintuitively obtain $G_- = 0$, resulting in the existence of the dark mode $\mathcal{B}_-$. Due to the appearance of the dark mode, all EPs and topological behavior are completely destroyed in practical quantum devices.

The underlying physics behind these counterintuitive phenomena is that the two phonon modes coupled to a common photon mode are hybridized into the dark and bright modes. This dark mode is fully decoupled from the system and, as a result, the thermal phonons concealed in the dark mode cannot be extracted to the bright mode, leading to the destruction of all the EPs and topological responses. Therefore, it is naturally to arise the question whether a general topological mechanism, which is completely immune to the dark mode, can be generated in quantum systems.

C. Dark-mode engineering

Previously established topological achievements are focused exclusively on the conventional scenarios where dark modes are entirely circumvented, owing to the fragility of topological responses due to these dark modes [S1, S2]. Nevertheless, the practical applicability of modern topological technologies has challenged such progresses by demonstrating that a universal approach must be explored for confronting this outstanding challenge posed by the dark modes, rather than evading it [S3–S12]. In view of its significance and urgency, utilizing a fundamentally distinct nonreciprocal topology immune to dark modes, as well as shielding both EPs and topological operations from dark-mode disturbances in practical devices, is highly desirable. Here we show how to address this long-standing challenge and reveal its counterintuitive immunity against dark modes. This occurs because of the synergy of topological operations [S1, S2] and synthetic magnetism [S13–S21], resulting in an exceptional transition between the $\mathcal{DMN}$ and $\mathcal{DMB}$ regimes in a well-controlled manner. Note that reconfigurable synthetic gauge fields have recently been reported based on the phase-dependent loop-coupled optomechanical platforms [S13–S21].

Now, we show in detail how the dark mode is flexibly engineered on demand by simply employing the synthetic magnetism (i.e., $\xi \neq 0$ and $\Theta \neq n\pi$). To demonstrate this, two superposition-phonon modes, associated with the synthetic magnetism, are introduced as $\tilde{\mathcal{B}}_+$ and $\tilde{\mathcal{B}}_-$, which are defined by

$$\tilde{\mathcal{B}}_+ = \mathcal{F}\delta b_1 - e^{i\Theta}\mathcal{K}\delta b_2, \tag{S13a}$$

$$\tilde{\mathcal{B}}_- = e^{-i\Theta}\mathcal{K}\delta b_1 + \mathcal{F}\delta b_2. \tag{S13b}$$

Then the system Hamiltonian in Eq. (S7) becomes

$$\mathcal{H}_{\rm lin} = -\Delta\delta a^\dagger\delta a + \tilde{\omega}_+\tilde{\mathcal{B}}_+^\dagger\tilde{\mathcal{B}}_+ + \tilde{\omega}_-\tilde{\mathcal{B}}_-^\dagger\tilde{\mathcal{B}}_- + (\tilde{G}_+^*\delta a\tilde{\mathcal{B}}_+^\dagger + \tilde{G}_+\tilde{\mathcal{B}}_+\delta a^\dagger) + (\tilde{G}_-^*\delta a\tilde{\mathcal{B}}_-^\dagger + \tilde{G}_-\tilde{\mathcal{B}}_-\delta a^\dagger), \tag{S14}$$

where the resonance frequencies $\tilde{\omega}_\pm$ and the coupling strengths $\tilde{G}_\pm$ are, respectively, defined as

$$\tilde{\omega}_\pm = \frac{1}{2}\Big(\omega_1 + \omega_2 \pm \sqrt{(\omega_1-\omega_2)^2 + 4\xi^2}\Big), \tag{S15}$$

and

$$\tilde{G}_+ = \mathcal{F}G_1 - e^{-i\Theta}\mathcal{K}G_2, \tag{S16a}$$

$$\tilde{G}_- = e^{i\Theta}\mathcal{K}G_1 + \mathcal{F}G_2, \tag{S16b}$$

with

$$\mathcal{F} = |\tilde{\omega}_- - \omega_1|/\sqrt{(\tilde{\omega}_- - \omega_1)^2 + \xi^2}, \tag{S17a}$$

$$\mathcal{K} = \xi\mathcal{F}/(\tilde{\omega}_- - \omega_1). \tag{S17b}$$

To illustrate the dark-mode engineering mechanism, we plot the redefined coupling $\tilde{G}_\pm$ as a function of the modulation phase Θ when $\omega_1 = \omega_2$ and $G_1 = G_2$, as shown in Fig. S1(c). We find that when $\Theta = n\pi$, a dark mode decoupled from the system emerges (i.e., $\tilde{G}_\pm = 0$), corresponding to the $\mathcal{DMN}$ regime. Counterintuitively, an effective coupling of the dark mode to the system can be flexibly achieved just by tuning $\Theta \neq n\pi$, resulting in the $\mathcal{DMB}$ regime. The fundamental physics driving these counterintuitive phenomena lies in the fact that a reconfigurable synthetic gauge field is built on demand by simply tuning the modulation phase Θ in the loop-coupled system, enabling an exceptional transition between the $\mathcal{DMN}$ and $\mathcal{DMB}$ regimes.

Beyond the above numerical simulations used to investigate the dark-mode engineering mechanism, we below further derive analytical expressions to explicitly reveal the dark-mode breaking process, providing deeper physical insight. Specifically, when the two mechanical modes are degeneracy in their resonance frequencies (i.e., $\omega_1 = \omega_2$), the effective optomechanical coupling strengths shown in Eq. (S16) can be simplified as

$$\tilde{G}_+ = (G_1 + e^{-i\Theta}G_2)/\sqrt{2}, \tag{S18a}$$

$$\tilde{G}_- = (G_2 - e^{i\Theta}G_1)/\sqrt{2}. \tag{S18b}$$

We perform a systematic analysis of dark-mode engineering, examining its dependence on both the modulation phase (Θ) and the optomechanical coupling strengths (G_1 and G_2), with particular focus on three representative cases.

(i) When the system operates in the symmetric-coupling case, i.e., $G_1 = G_2 = G$, the following relationship holds:

$$\tilde{G}_+ = G(1 + e^{-i\Theta})/\sqrt{2}, \tag{S19a}$$

$$\tilde{G}_- = G(1 - e^{i\Theta})/\sqrt{2}. \tag{S19b}$$

We clearly see from Eq. (S19) that, when $\Theta = n\pi$ (where n is an integer), one of the two hybrid phonon modes is completely decoupled from the cavity mode, indicating the emergence of the dark mode. In this case, thermal excitations stored in the dark mode cannot be extracted through the optomechanical-cooling channel or topological operations. In general cases of $\Theta \neq n\pi$, this dark mode can be completely broken and then, both quantum collective ground-state preparation and TPT become accessible under proper parameter conditions.

(ii) For an even-integer phase condition (i.e., $\Theta = n\pi$ where n is even), Eq. (S18) simplifies to

$$\tilde{G}_+ = (G_1 + G_2)/\sqrt{2}, \tag{S20a}$$

$$\tilde{G}_- = (G_2 - G_1)/\sqrt{2}. \tag{S20b}$$

As evident from Eq. (S20), the mode $\tilde{\mathcal{B}}_-$ enters a dark state when $G_1 = G_2$, while imbalanced coupling strengths ($G_1 \neq G_2$) completely break this dark mode. These findings establish that simultaneous ground-state cooling and TPT require a broken coupling symmetry ($G_2/G_1 \neq 1$).

(iii) For an odd-integer phase matching (i.e., $\Theta = n\pi$ where n is an odd), Eq. (S18) transforms to

$$\tilde{G}_+ = (G_1 - G_2)/\sqrt{2}, \tag{S21a}$$

$$\tilde{G}_- = (G_2 + G_1)/\sqrt{2}. \tag{S21b}$$

Equation (S21) establishes that the $\tilde{\mathcal{B}}_+$ mode becomes a dark mode under symmetric coupling (i.e., $G_1 = G_2$), with a complete breaking of this dark mode occurring for asymmetric coupling (i.e., $G_1 \neq G_2$). This analysis demonstrates that the broken symmetry in optomechanical coupling (i.e., $G_2/G_1 \neq 1$) enables the concurrent quantum collective ground-state preparation and TPT.

II. EFFECTIVE NON-HERMITIAN HAMILTONIAN AND ITS EXCEPTIONAL POINT

In this section, we show in detail (i) an effective non-Hermitian Hamiltonian; (ii) an exceptional point (EP); (iii) malfunction and function of the EP; (iv) inactivation and activation of topological operations; (v) eigenvalue distributions and transient behaviors around the EP.

A. Effective non-Hermitian Hamiltonian

The solution of Eq. (S6) can be used to solve both TPB and TPT, which is achieved by transforming all the system variables into the frequency domain by the Fourier transformation. Physically, this method can be utilized for a better understanding of the optical modifications of vibrational susceptibilities.

We apply the Fourier transformation for operators o and their conjugates $o^\dagger$, i.e.,

$$o(t) = \frac{1}{\sqrt{2\pi}} \int_{-\infty}^{\infty} e^{i\omega t} o(\omega)\, d\omega, \quad \text{and} \quad o^\dagger(t) = \frac{1}{\sqrt{2\pi}} \int_{-\infty}^{\infty} e^{-i\omega t} o^\dagger(\omega)\, d\omega, \tag{S22}$$

for $o = a$, b_1, and b_2. By executing the Fourier transformation using Eq. (S22), the equations of motion in Eq. (S6) can be expressed in the frequency domain as:

$$-i\omega\delta a(\omega) = -\left(\frac{\kappa}{2} - i\Delta\right)\delta a(\omega) - iG_1\delta z_1(\omega) - iG_2\delta z_2(\omega), \tag{S23a}$$

$$-i\omega\delta a^\dagger(\omega) = -\left(\frac{\kappa}{2} + i\Delta\right)\delta a^\dagger(\omega) + iG_1^*\delta z_1^\dagger(\omega) + iG_2^*\delta z_2^\dagger(\omega), \tag{S23b}$$

$$-i\omega\delta b_1(\omega) = -\left(\frac{\gamma_1}{2} + i\omega_1\right)\delta b_1(\omega) - i\left[G_1^*\delta a(\omega) + G_1\delta a^\dagger(\omega)\right] - i\xi e^{i\Theta}\delta b_2(\omega) + \sqrt{\gamma_1}\eta_1, \tag{S23c}$$

$$-i\omega\delta b_2(\omega) = -\left(\frac{\gamma_2}{2} + i\omega_2\right)\delta b_2(\omega) - i\left[G_2^*\delta a(\omega) + G_2\delta a^\dagger(\omega)\right] - i\xi e^{-i\Theta}\delta b_1(\omega) + \sqrt{\gamma_2}\eta_2. \tag{S23d}$$

Using Eq. (S23), we subsequently have the following equations:

$$\left[\frac{\kappa}{2} - i(\omega + \Delta)\right]\delta a(\omega) = -iG_1\delta z_1(\omega) - iG_2\delta z_2(\omega), \tag{S24a}$$

$$\left[\frac{\kappa}{2} + i(\Delta - \omega)\right]\delta a^\dagger(\omega) = iG_1^*\delta z_1^\dagger(\omega) + iG_2^*\delta z_2^\dagger(\omega), \tag{S24b}$$

$$\left[\frac{\gamma_1}{2} - i(\omega - \omega_1)\right]\delta b_1(\omega) = -i\left[G_1^*\delta a(\omega) + G_1\delta a^\dagger(\omega)\right] - i\xi e^{i\Theta}\delta b_2(\omega) + \sqrt{\gamma_1}\eta_1, \tag{S24c}$$

$$\left[\frac{\gamma_2}{2} - i(\omega - \omega_2)\right]\delta b_2(\omega) = -i\left[G_2^*\delta a(\omega) + G_2\delta a^\dagger(\omega)\right] - i\xi e^{-i\Theta}\delta b_1(\omega) + \sqrt{\gamma_2}\eta_2, \tag{S24d}$$

where we define an optical susceptibility $\chi(\omega)$ as

$$\chi(\omega) = \left[\frac{\kappa}{2} - i(\omega + \Delta)\right]^{-1}. \tag{S25}$$

Therefore, one can easily find

$$\delta a(\omega) = -iG_1\chi(\omega)\left(\delta b_1^\dagger + \delta b_1\right) - iG_2\chi(\omega)\left(\delta b_2^\dagger + \delta b_2\right), \tag{S26}$$

where the position operators z_j are defined as

$$z_j = b_j^\dagger + b_j. \tag{S27}$$

Subsequently, we substitute Eq. (S27) into Eq. (S26), and obtain

$$\left[\frac{\kappa}{2} + i(\Delta - \omega)\right]\delta a^\dagger(\omega) = iG_1^*\delta z_1^\dagger + iG_2^*\delta z_2^\dagger = iG_1^*\delta z_1 + iG_2^*\delta z_2. \tag{S28}$$

Consequently, we can easily find

$$\delta a^\dagger(\omega) = iG_1^*\chi^*(-\omega)\,\delta z_1 + iG_2^*\chi^*(-\omega)\,\delta z_2, \tag{S29}$$

where the optical susceptibilities are defined as

$$\chi(\omega) = \left[\frac{\kappa}{2} - i(\omega + \Delta)\right]^{-1}, \tag{S30a}$$

$$\chi^*(\omega) = \left[\frac{\kappa}{2} + i(\omega + \Delta)\right]^{-1}, \tag{S30b}$$

$$\chi(-\omega) = \left[\frac{\kappa}{2} - i(-\omega + \Delta)\right]^{-1}, \tag{S30c}$$

$$\chi^*(-\omega) = \left[\frac{\kappa}{2} + i(\Delta - \omega)\right]^{-1}. \tag{S30d}$$

Therefore, we have:

$$\delta a(\omega) = -i\alpha_1\chi(\omega)\left(\delta b_1^\dagger + \delta b_1\right) - i\alpha_2\chi(\omega)\left(\delta b_2^\dagger + \delta b_2\right), \tag{S31a}$$

$$\delta a^\dagger(\omega) = i\alpha_1^*\chi^*(-\omega)\left(\delta b_1^\dagger + \delta b_1\right) + i\alpha_2^*\chi^*(-\omega)\left(\delta b_2^\dagger + \delta b_2\right). \tag{S31b}$$

Next, the expressions of δa and $\delta a^\dagger$, which are shown in Eqs. (S31), are substituted into Eqs. (S24c) and (S24d), and, then, we obtain:

$$\begin{aligned}\left[\frac{\gamma_1}{2} - i(\omega - \omega_1)\right]\delta b_1(\omega) =& -iG_1^*\left[-iG_1\chi(\omega)\left(\delta b_1^\dagger + \delta b_1\right) - iG_2\chi(\omega)\left(\delta b_2^\dagger + \delta b_2\right)\right] \\ & - iG_1\left[iG_1^*\chi^*(-\omega)\left(\delta b_1^\dagger + \delta b_1\right) + iG_2^*\chi^*(-\omega)\left(\delta b_2^\dagger + \delta b_2\right)\right] - i\xi e^{i\Theta}\delta b_2 + \sqrt{\gamma_1}\eta_1,\end{aligned} \tag{S32a}$$

$$\begin{aligned}\left[\frac{\gamma_2}{2} - i(\omega - \omega_2)\right]\delta b_2(\omega) =& -iG_2^*\left[-iG_1\chi(\omega)\left(\delta b_1^\dagger + \delta b_1\right) - iG_2\chi(\omega)\left(\delta b_2^\dagger + \delta b_2\right)\right] \\ & - iG_2\left[iG_1^*\chi^*(-\omega)\left(\delta b_1^\dagger + \delta b_1\right) + iG_2^*\chi^*(-\omega)\left(\delta b_2^\dagger + \delta b_2\right)\right] - i\xi e^{-i\Theta}\delta b_1 + \sqrt{\gamma_2}\eta_2,\end{aligned} \tag{S32b}$$

$$\begin{aligned}\left[\frac{\gamma_1}{2} - i(\omega - \omega_1)\right]\delta b_1(\omega) =& G_1G_1^*\left[-\chi(\omega) + \chi^*(-\omega)\right]\left(\delta b_1^\dagger + \delta b_1\right) \\ & + \left[-G_1^*G_2\chi(\omega) + G_1G_2^*\chi^*(-\omega)\right]\left(\delta b_2^\dagger + \delta b_2\right) - i\xi e^{i\Theta}\delta b_2 + \sqrt{\gamma_1}\eta_1,\end{aligned} \tag{S32c}$$

$$\begin{aligned}\left[\frac{\gamma_2}{2} - i(\omega - \omega_2)\right]\delta b_2(\omega) =& \left[-G_2^*G_1\chi(\omega) + G_2G_1^*\chi^*(-\omega)\right]\left(\delta b_1^\dagger + \delta b_1\right) \\ & + \left[-G_2^*G_2\chi(\omega) + G_2G_2^*\chi^*(-\omega)\right]\left(\delta b_2^\dagger + \delta b_2\right) - i\xi e^{-i\Theta}\delta b_1 + \sqrt{\gamma_2}\eta_2.\end{aligned} \tag{S32d}$$

We here safely drop the counter-rotating terms $\delta b_j^\dagger$ and the mechanical drive terms η_j. These terms are not necessary for the physical model that operates far from the ultrastrong coupling regime. This is because we drive the system into a particular initial state, turn off the drive, and then, focus on the evolution of the system without any mechanical drive. Consequently, Eqs. (S32) become:

$$\left[\frac{\gamma_1}{2} - i(\omega - \omega_1)\right]\delta b_1(\omega) = G_1G_1^*\left[-\chi(\omega) + \chi^*(-\omega)\right]\delta b_1(\omega) + \left[-G_1^*G_2\chi(\omega) + G_1G_2^*\chi^*(-\omega)\right]\delta b_2(\omega) - i\xi e^{i\Theta}\delta b_2, \tag{S33a}$$

$$\left[\frac{\gamma_2}{2} - i(\omega - \omega_2)\right]\delta b_2(\omega) = \left[-G_1G_2^*\chi(\omega) + G_1^*G_2\chi^*(-\omega)\right]\delta b_1(\omega) + G_2^*G_2\left[-\chi(\omega) + \chi^*(-\omega)\right]\delta b_2(\omega) - i\xi e^{-i\Theta}\delta b_1. \tag{S33b}$$

Subsequently, using Eqs. (S33), one can easily obtain:

$$\left[\frac{\gamma_1}{2} - i(\omega - \omega_1)\right]\delta b_1(\omega) = |G_1|^2\left[\chi^*(-\omega) - \chi(\omega)\right]\delta b_1(\omega) + G_1^*G_2\left[\chi^*(-\omega) - \chi(\omega)\right]\delta b_2(\omega) - i\xi e^{i\Theta}\delta b_2, \tag{S34a}$$

$$\left[\frac{\gamma_2}{2} - i(\omega - \omega_2)\right]\delta b_2(\omega) = G_1^*G_2\left[\chi^*(-\omega) - \chi(\omega)\right]\delta b_1(\omega) + |G_2|^2\left[\chi^*(-\omega) - \chi(\omega)\right]\delta b_2(\omega) - i\xi e^{-i\Theta}\delta b_1. \tag{S34b}$$

Equation (S34) can be rewritten in a standard form:

$$-i\omega\delta b_1(\omega) = -\left(\frac{\gamma_1}{2} + i\omega_1\right)\delta b_1(\omega) - i\xi e^{i\Theta}\delta b_2(\omega) + |G_1|^2\left[\chi^*(-\omega) - \chi(\omega)\right]\delta b_1(\omega) + G_1^*G_2\left[\chi_c^*(-\omega) - \chi_c(\omega)\right]\delta b_2(\omega), \tag{S35a}$$

$$-i\omega\delta b_2(\omega) = -\left(\frac{\gamma_2}{2} + i\omega_2\right)\delta b_2(\omega) - i\xi e^{-i\Theta}\delta b_1(\omega) + G_1^*G_2\left[\chi^*(-\omega) - \chi(\omega)\right]\delta b_1(\omega) + |G_2|^2\left[\chi^*(-\omega) - \chi(\omega)\right]\delta b_2(\omega). \tag{S35b}$$

Thus, based on Eq. (S35), the matrix form can be given as

$$-i\omega\begin{pmatrix}\delta b_1(\omega)\\ \delta b_2(\omega)\end{pmatrix} = \begin{pmatrix}-\left(\frac{\gamma_1}{2} + i\omega_1\right) & -i\xi e^{i\Theta}\\ -i\xi e^{-i\Theta} & -\left(\frac{\gamma_2}{2} + i\omega_2\right)\end{pmatrix}\begin{pmatrix}\delta b_1(\omega)\\ \delta b_2(\omega)\end{pmatrix} + \begin{pmatrix}|G_1|^2 & G_1^*G_2\\ G_1^*G_2 & |G_2|^2\end{pmatrix}\left[\chi^*(-\omega) - \chi(\omega)\right]\begin{pmatrix}\delta b_1(\omega)\\ \delta b_2(\omega)\end{pmatrix}. \tag{S36}$$

A single-mode optomechanical intrinsic self-energy, in the traditional standard optomechanical systems, can be give as

$$\sum(\omega) = i\left|G_j\right|^2\left[\chi^*(-\omega) - \chi(\omega)\right]. \tag{S37}$$

Note that $\sum(\omega)$ is often called the optomechanical intrinsic "self-energy", and represents the optical modification of the mechanical resonance. This arises from the self-interaction occurring via the dynamical system formed by the optics/mechanics. From the definition of $\sum(\omega)$, we see that it is a complex quantity depending on the laser power and detuning [through its dependence on incavity photon numbers $\bar{a}$ and and optical susceptibly $\chi(\omega)$]. We also note here that the dependence on ω comes only through the cavity susceptibility, which varies with ω on a scale of κ. Since we are considering only a weak interaction, we can assume that the width of the mechanical resonance will be significantly less than κ. Thus, we can assume that $\chi(\omega)$ and hence $\sum(\omega)$ are constant with respect to ω over the relevant mechanical bandwidth. Therefore, we can eliminate the frequency dependence and simply evaluate the self-energy at the mechanical frequency: $\sum(\omega) \approx \sum(\omega_0) = \sum$.

By inspecting the appearance of $\sum$ in the effective susceptibility, we see that the real part of $\sum$ corresponds to a shift in the mechanical frequency ("optical spring"), while the imaginary part results in a change in the effective damping rate of the oscillator ("optical damping"). This dynamical backaction is the mechanism by which one is able to control the motion in an optomechanical system, by exploiting and controlling the radiation pressure force. We now explore this control in a more detail, to better understand its limitations and tunability.

Specifically, Eq. (S37) can be rewritten as

$$\sum(\omega) = \begin{pmatrix} i\left|G_1\right|^2 & i\left|G_1^* G_2\right| \\ i\left|G_1^* G_2\right| & i\left|G_2\right|^2 \end{pmatrix}\left[\chi^*(-\omega) - \chi(\omega)\right] = \begin{pmatrix} -ig_1^2\sigma & -ig_1 g_2\sigma \\ -ig_1 g_2\sigma & -ig_2^2\sigma \end{pmatrix}, \tag{S38}$$

where the complex mechanical susceptibilities, i.e., σ introduced by the laser driving of the system, can be defined as

$$\sigma = \frac{P\kappa_{\text{in}}}{\hbar\omega\left[\left(\frac{\kappa}{2}\right)^2 + \Delta^2\right]}\left[\frac{1}{\frac{\kappa}{2} - i(\omega_0 + \Delta)} - \frac{1}{\frac{\kappa}{2} + i(-\omega_0 + \Delta)}\right]. \tag{S39}$$

Now, we obtain

$$-i\omega\begin{pmatrix} \delta b_1(\omega) \\ \delta b_2(\omega) \end{pmatrix} = \begin{pmatrix} -\left(\frac{\gamma_1}{2} + i\omega_1\right) & -i\xi e^{i\Theta} \\ -i\xi e^{-i\Theta} & -\left(\frac{\gamma_2}{2} + i\omega_2\right) \end{pmatrix}\begin{pmatrix} \delta b_1(\omega) \\ \delta b_2(\omega) \end{pmatrix} - i\sum(\omega)\begin{pmatrix} \delta b_1(\omega) \\ \delta b_2(\omega) \end{pmatrix}. \tag{S40}$$

Subsequently, Eq. (S40) is safely rewritten in a matrix form defined:

$$-i\omega\mathbf{B}(\omega) = -\begin{pmatrix} \left(\frac{\gamma_1}{2} + i\omega_1\right) & i\xi e^{i\Theta} \\ i\xi e^{-i\Theta} & \left(\frac{\gamma_2}{2} + i\omega_2\right) \end{pmatrix}\mathbf{B}(\omega) - i\sum(\omega)\mathbf{B}(\omega), \tag{S41}$$

where the matrix $\mathbf{B}(\omega)$ is obtained as

$$\mathbf{B}(\omega) = \begin{pmatrix} \delta b_1(\omega) \\ \delta b_2(\omega) \end{pmatrix}. \tag{S42}$$

Before moving back to the time domain, we note that $\sum(\omega)$ varies on the scale of κ, whereas the mechanical modes are susceptible to the drives only within their linewidths, which is substantially smaller than κ, by our assumption.

Therefore, it is both safe and sufficient to consider the following assumptions:

$$\sum(\omega) \approx \sum(\omega_1) \approx \sum(\omega_2) \equiv \sum, \tag{S43}$$

where

$$\sum = \sum(\omega_0) = \sum\left(\frac{\omega_1 + \omega_2}{2}\right), \tag{S44}$$

for

$$\omega_0 = (\omega_1 + \omega_2)/2. \tag{S45}$$

We note that the vibrational modes are also assumed to be nearly degenerate. Therefore, owing to the fact that $\sum$ is not a function of ω, we can easily move back to the time domain, to find the following equation:

$$\dot{\mathbf{B}}(t) = -\begin{pmatrix} \left(\frac{\gamma_1}{2} + i\omega_1\right) & i\xi e^{i\Theta} \\ i\xi e^{-i\Theta} & \left(\frac{\gamma_2}{2} + i\omega_2\right) \end{pmatrix}\mathbf{B}(t) - i\sum\mathbf{B}(t). \tag{S46}$$

Mathematically, we adiabatically eliminate the optical mode and then, an effective Hamiltonian only for two phonon modes (i.e., b_1 and b_2) can be obtained as

$$i\dot{\mathbf{B}}(t) = \mathcal{H}_{\text{eff}}\mathbf{B}(t), \tag{S47}$$

with

$$\mathcal{H}_{\text{eff}} = \begin{pmatrix} \omega_1 - \frac{i\gamma_1}{2} - ig_1^2\sigma & \xi e^{i\Theta} - ig_1g_2\sigma \\ \xi e^{-i\Theta} - ig_1g_2\sigma & \omega_2 - \frac{i\gamma_2}{2} - ig_2^2\sigma \end{pmatrix}, \tag{S48}$$

The simplified complex vibrational susceptibility σ, which is introduced by the laser driving and based on Eq. (S39), can be defined as

$$\sigma = \frac{P\kappa_{\text{in}}\left[\chi_{R,L}(\omega_0) - \chi^*(-\omega_0)\right]}{\hbar\omega\left[(\kappa/2)^2 + \Delta^2\right]}, \tag{S49}$$

where the optical susceptibility $\chi(\omega_0)$ is defined as

$$\chi(\omega_0) = \left[\frac{\kappa}{2} - i(\omega_0 + \Delta)\right]^{-1}. \tag{S50}$$

Below, an exceptional point (EP) of the physical system will be derived in detail, and the TPT performance using the Hamiltonian $\mathcal{H}_{\text{eff}}$ in Eq. (S48) will be analyzed in detail.

B. Exceptional point

In this section, we focus on a three-mode optomechanical device consisting of two phonon modes, each of which is linearly coupled to a common photon mode through radiation-pressure interactions. In addition, the two phonon modes are coupled to each other via a phase-dependent phonon-hopping interaction, and this interaction together with the optomechanical couplings form a phase-dependent loop-coupled configuration, which can induce synthetic magnetism for achieving dark-mode engineering.

Adiabatically eliminating the photon mode leads to a tunable effective interaction between the two phonon modes, and this effective interaction, which induces an EP, is generated by the driving field of the system. In the following detailed analysis, we can safely eliminate the common evolution, with a mean frequency ω_0 [see Eq. (S45)] of the two phonon modes and an average damping rate Γ of the two phonon modes defined as

$$\Gamma = (\gamma_1 + \gamma_2)/2. \tag{S51}$$

Note that the parameters ω_j and γ_j are replaced with the redefined parameters ω_0, Ω, Γ, and γ. Therefore, the effective non-Hermitian Hamiltonian $\mathcal{H}_{\text{eff}}$, which is given in Eq. (S48), becomes

$$\mathcal{H}_{\text{eff}} = \begin{pmatrix} \omega_0 - i\frac{\Gamma}{2} - \Omega - i\frac{\gamma}{2} - ig_1^2\sigma & \xi e^{i\Theta} - ig_1g_2\sigma \\ \xi e^{-i\Theta} - ig_1g_2\sigma & \omega_0 - i\frac{\Gamma}{2} + \Omega + i\frac{\gamma}{2} - ig_2^2\sigma \end{pmatrix}, \tag{S52}$$

where Ω and γ are defined as:

$$\Omega = (\omega_2 - \omega_1)/2, \tag{S53}$$

and

$$\gamma = (\gamma_1 - \gamma_2)/2. \tag{S54}$$

Subsequently, we easily obtain the following equations:

$$\begin{aligned} i\frac{d}{dt}\begin{pmatrix} b_1(t) \\ b_2(t) \end{pmatrix} &= \begin{pmatrix} \omega_0 - i\frac{\Gamma}{2} - \Omega - i\frac{\gamma}{2} - ig_1^2\sigma & \xi e^{i\Theta} - ig_1g_2\sigma \\ \xi e^{-i\Theta} - ig_1g_2\sigma & \omega_0 - i\frac{\Gamma}{2} + \Omega + i\frac{\gamma}{2} - ig_2^2\sigma \end{pmatrix}\begin{pmatrix} b_1(t) \\ b_2(t) \end{pmatrix}, \\ &= \begin{pmatrix} \omega_0 - i\frac{\Gamma}{2} & 0 \\ 0 & \omega_0 - i\frac{\Gamma}{2} \end{pmatrix}\begin{pmatrix} b_1(t) \\ b_2(t) \end{pmatrix} + \begin{pmatrix} -\Omega - i\frac{\gamma}{2} - ig_1^2\sigma & \xi e^{i\Theta} - ig_1g_2\sigma \\ \xi e^{-i\Theta} - ig_1g_2\sigma & \Omega + i\frac{\gamma}{2} - ig_2^2\sigma \end{pmatrix}\begin{pmatrix} b_1(t) \\ b_2(t) \end{pmatrix}, \\ &= \begin{pmatrix} \omega_0 - i\frac{\Gamma}{2} & 0 \\ 0 & \omega_0 - i\frac{\Gamma}{2} \end{pmatrix}\begin{pmatrix} b_1(t) \\ b_2(t) \end{pmatrix} + i\frac{d}{dt}\begin{pmatrix} b_+(t) \\ b_-(t) \end{pmatrix}, \end{aligned} \tag{S55}$$

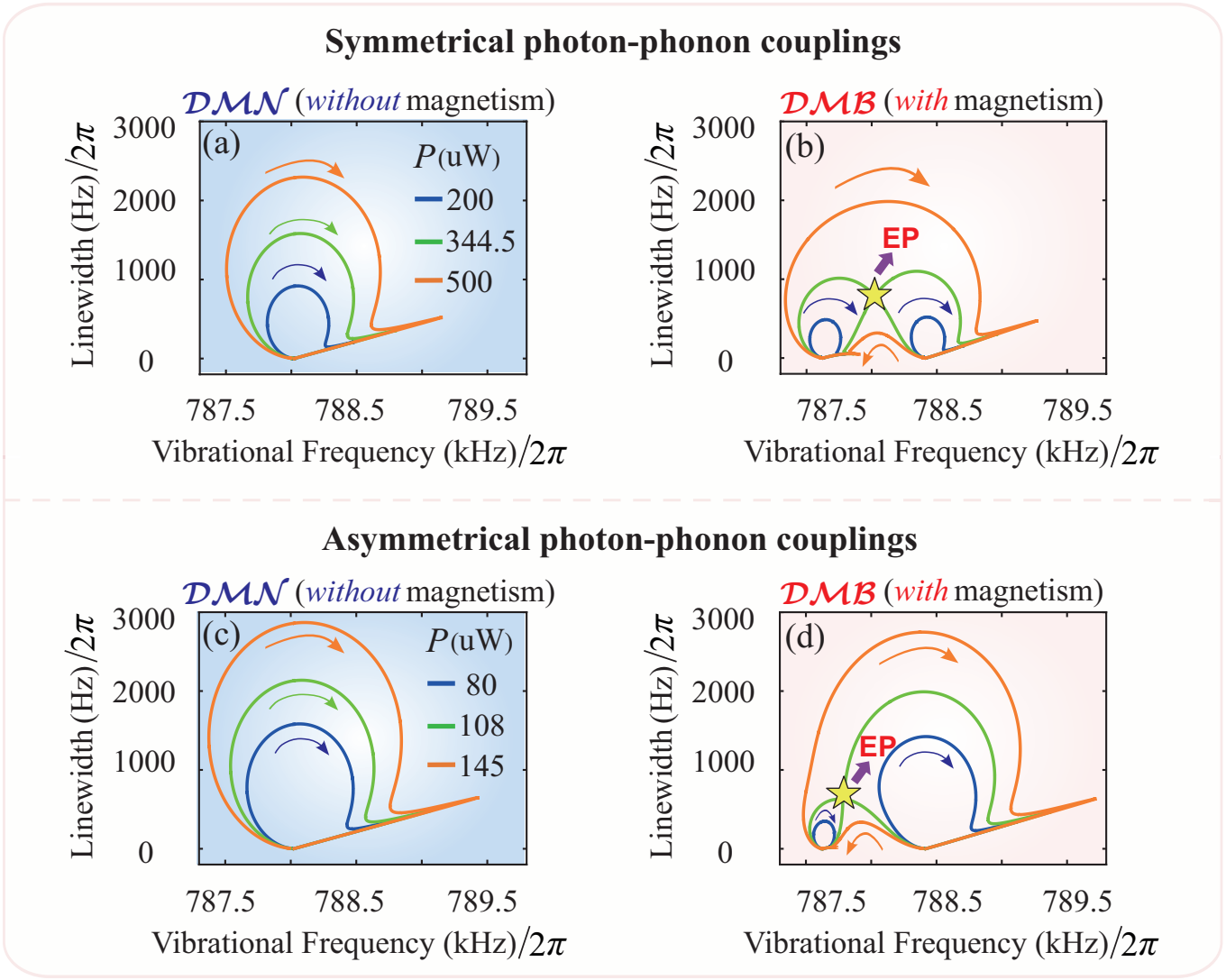

FIG. S2: (a,b) For the symmetrical optomechanical-coupling case ($g_2 = g_1$), mechanical linewidths and resonance frequencies of both the dark and bright modes versus the driving power P and the driving detuning $\Delta \in [-1800\ \text{kHz}, 0]$, when the system operates in (a) the $\mathcal{DMN}$ ($\xi = 0$) and (b) $\mathcal{DMB}$ ($\xi/\omega_1 = 5\times10^{-4}$ and $\Theta/\pi = 1/2$) regimes. (c,d) For the asymmetrical optomechanical-coupling case ($g_2 = 2.76g_1$), mechanical linewidths and resonance frequencies of both the dark and bright modes versus the driving power P and detuning $\Delta \in [-1800\ \text{kHz}, 0]$, when the system operates in (c) the $\mathcal{DMN}$ ($\xi = 0$) and (d) $\mathcal{DMB}$ ($\xi/\omega_1 = 5\times10^{-4}$ and $\Theta/\pi = 1/9$) regimes.

where

$$i\frac{d}{dt}\begin{pmatrix} b_+(t) \\ b_-(t) \end{pmatrix} = \begin{pmatrix} -\Omega - i\frac{\gamma}{2} - ig_1^2\sigma & \xi e^{i\Theta} - ig_1g_2\sigma \\ \xi e^{-i\Theta} - ig_1g_2\sigma & \Omega + i\frac{\gamma}{2} - ig_2^2\sigma \end{pmatrix}\begin{pmatrix} b_1(t) \\ b_2(t) \end{pmatrix}. \tag{S56}$$

We then obtain the eigenvalues of the effective non-Hermitian Hamiltonian, shown in Eq. (S52), as

$$\lambda_\mp = -\frac{i}{2}\left(g_1^2 + g_2^2\right)\sigma \mp \lambda, \tag{S57}$$

where the parameter λ is defined as

$$\lambda = i\sqrt{\left\{g_1^2g_2^2\sigma^2 + \frac{1}{4}\left[\gamma + \left(g_1^2 - g_2^2\right)\sigma\right]^2 - \Omega^2 - \xi^2\right\} - i\left\{\Omega\left[\gamma + \left(g_1^2 - g_2^2\right)\sigma\right] - 2g_1g_2\xi\sigma\cos\Theta\right\}}. \tag{S58}$$

Therefore, we obtain:

$$\tilde{\lambda}_\mp = \omega_0 - \frac{i\Gamma}{2} - \frac{i}{2}\left(g_1^2 + g_2^2\right)\sigma \mp \lambda. \tag{S59}$$

Just by simply tuning the complex vibrational susceptibilities σ, the system possesses an EP. Thus, one needs to control over both $\mathrm{Re}(\sigma)$ and $\mathrm{Im}(\sigma)$. The imaginary and real parts of the complex eigenvalues of the two phononic normal modes $\mathcal{B}_+$ and $\mathcal{B}_-$ are the mechanical linewidths $\gamma_\pm(\Delta, P) = -2\mathrm{Im}(\lambda_\pm)$ and the mechanical resonance frequencies $\omega_\pm(\Delta, P) = \mathrm{Re}(\lambda_\pm)$, respectively. Note that in our model, the control of the optomechanical system is achieved by a separate laser, and its driving power P and driving detuning Δ are set by an acousto-optic modulator. We can measure the vibration spectra of the phonon modes as functions of the driving detuning Δ and the driving power P, so that the presence of the EP in our system can be accurately established. In addition, these mechanical spectra are acquired by driving the motions and monitoring its response via a heterodyne signal. We fit each spectrum to determine the two motional damping rates, $\gamma_\pm(\Delta, P)$, and the two vibrational resonance frequencies, $\omega_\pm(\Delta, P)$. Note that the subscripts "±" refer to the phononic normal modes, as introducing the optical field into the physical system.

Now, in both the $\mathcal{DMN}$ and $\mathcal{DMB}$ regimes, we show measurements of both the real and imaginary parts of the corresponding complex eigenvalues for the two vibrational normal modes over a narrow range of the driving detuning Δ and the driving power P, which are centred at Δ_{EP} and P_{EP}. The parameters Δ_{EP} and P_{EP} denote the parameter position of the EP. These measurements show the characteristic features of an EP. In the vicinity of this point, they exhibit the same structure as the Riemann sheets of a complex square-root function. The surfaces are such that if the driving-laser detuning Δ and the driving-laser power P were varied to execute a single closed loop, the resulting smooth evolution on the eigenvalue manifold would return to its starting point only if the loop does not enclose the EP. By contrast, a loop enclosing the EP would result in a trajectory starting on one sheet, but ending on the other.

In addition, the complex eigenvalues of the two phononic normal modes are shown in Fig. S2, by considering the symmetrical and asymmetrical optomechanical coupling cases. Specifically, we plot the motional decay rates [$\gamma_\pm(\Delta, P)$, see the vertical axis] and the vibrational resonance frequencies [$\omega_\pm(\Delta, P)$, see the horizontal axis] of the two phononic normal modes as functions of the driving detuning Δ and the driving laser power P, when the system operates in both the $\mathcal{DMN}$ and $\mathcal{DMB}$ regimes. Note that the values of the driving laser power P are described by different colors, and the eigenvalues of the system are varied with the driving detuning $\Delta \in [-1800\ \mathrm{kHz}, 0]$ at a fixed P.

When considering the cases of symmetrical and asymmetrical photon-phonon couplings, for the $\mathcal{DMN}$ regime, we show that despite the continuous evolution of the mechanical spectra with system parameters, the EP vanishes at both low and high laser powers, owing to the emergence of the dark mode, as shown in Figs. S2(a) and S2(c). Counterintuitively, when transitioning to the $\mathcal{DMB}$ regime, we find from Figs. S2(b) and S2(d) that for a lower value of the driving-laser power P, each eigenvalue follows an enclosed path, which begins and ends at the same point, and that for a higher value of the driving power P, both eigenvalues follow open paths, each starting at the ending point of the other, indicating the emergence of the EP because of breaking the dark mode.

In particular, we reveal that the EP (see the yellow star in Fig. S2), where the eigenstates coalesce, occurs by just tuning the laser power P and the driving detuning Δ. More specifically, we see from Eqs. (S48) and (S61) that in the resolved-sideband regime (i.e., $\kappa < \omega_0$), both reaching and encircling the EP require just to tune the driving power P and the driving detuning Δ, without the need of any complicated arrangements [S22]. This is due to the fact that the parameters P and Δ in our system can be easily steered in situ with timing accuracy, a high-precision degree, and dynamic range.

C. Malfunction and function of the exceptional point

Nontrivial topology is mainly governed by non-Hermitian degeneracies [S22–S39] and has led to a various of counterintuitive and fascinating topological properties by adiabatically encircling an EP in parameter spaces, e.g., chiral phase accumulation [S40, S41], non-adiabatic jumps [S42, S43], and nonreciprocal TPT or mode conversion [S1, S2, S44–S52]. These topological phenomena, however, are generally destroyed by dark modes naturally decoupled from the system, which results in a complete deactivation of both EPs and topological operations. Specifically, the TPT and mode switching can always happen when executing adiabatic closed paths enclosing an EP [S1, S2]. Surprisingly, once dark modes are possessed by the system, both the mode conversion and TPT between dark and bright modes are unfeasible regardless of the adjustment of adiabatic trajectories and system parameters, due to the dark-mode-induced destruction on topological operations and EPs.

In this section, we show how to address this long-standing challenge and achieve a profoundly different EP with a counterintuitive immunity against dark modes. This occurs because of the synergy of topological operations [S1, S2] and synthetic magnetism [S13–S21], resulting in an exceptional transition between the $\mathcal{DMN}$ and $\mathcal{DMB}$ regimes in a well-controlled manner. Note that a reconfigurable synthetic gauge field has recently been demonstrated in phase-dependent loop-coupled optomechanical configurations [S13–S21]. Specifically, we adiabatically eliminate the photon mode, and obtain an effective Hamiltonian for the two phonon modes, i.e.,

$$\mathcal{H}_{\mathrm{eff}} = \begin{pmatrix} \omega_1 - \frac{i\gamma_1}{2} - ig_1^2\sigma & \xi e^{i\Theta} - ig_1g_2\sigma \\ \xi e^{-i\Theta} - ig_1g_2\sigma & \omega_2 - \frac{i\gamma_2}{2} - ig_2^2\sigma \end{pmatrix}, \tag{S60}$$

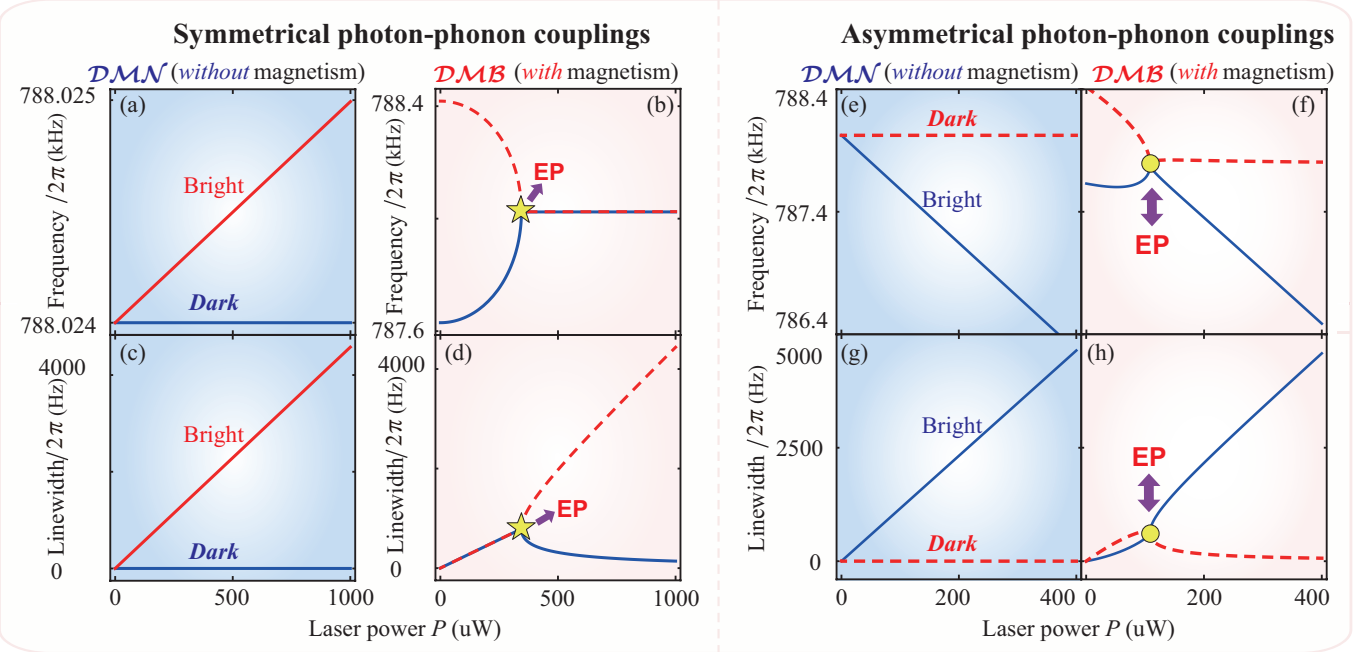

FIG. S3: (a-d) For the symmetrical optomechanical-coupling case ($g_2 = g_1$), (a,b) the resonance frequencies and (c,d) the decay rates of both the dark and bright modes versus the laser power P in (a,c) $\mathcal{DMN}$ ($\xi = 0$) and (b,d) $\mathcal{DMB}$ ($\xi/\omega_1 = 5 \times 10^{-4}$ and $\Theta/\pi = 1/2$) regimes, when $\Delta/2\pi = -783$ kHz. (e-h) For the asymmetrical optomechanical-coupling case ($g_2 = 2.76g_1$), (e,f) the resonance frequencies and (g,h) the mechanical linewidths of both the dark and bright modes versus the driving laser power P in (e,g) the $\mathcal{DMN}$ ($\xi = 0$) and (f,h) $\mathcal{DMB}$ ($\xi/\omega_1 = 5 \times 10^{-4}$ and $\Theta/\pi = 1/9$) regimes, when $\Delta/2\pi = -847.74$ kHz.

where the laser driving induces a complex motional susceptibility σ, which is defined as

$$\sigma = \frac{P\kappa_{\rm in}[\chi(\omega_0) - \chi^*(-\omega_0)]}{\hbar\omega_L[(\kappa/2)^2 + \Delta^2]}, \tag{S61}$$

with the driving detuning $\Delta = \omega_L - \omega_c$ and an optical susceptibility $\chi(\omega_0) = [\kappa/2 - i(\omega_0 + \Delta)]^{-1}$ for $\omega_0 = (\omega_1 + \omega_2)/2$. By tuning σ, the EP is easily reached, needing to control over both Im(σ) and Re(σ). Physically, the imaginary and real parts of the corresponding complex eigenvalues are the mechanical spectral linewidths and resonance frequencies, respectively. It is enough to tune P and Δ for reaching and encircling this EP, because these parameters are easily manipulated in situ with a high-precision degree, timing accuracy, and dynamic range [S1].

For elucidating the effect of the dark mode on the EP, the mechanical spectra are plotted as functions of Δ and P in both the $\mathcal{DMN}$ and $\mathcal{DMB}$ regimes, when the system operates in the symmetrical or asymmetrical optomechanical-coupling case, as shown in Fig. S2. We reveal in the $\mathcal{DMN}$ regime that for either lower or higher power of the laser, the mechanical spectrum on the dark mode remains invariant under the parameter evolution. However, the eigenvalue of the bright mode always follows an enclosed trajectory, which begins and ends at the same point, indicating the vanishing of the EP due to the dark mode [see Figs. S2(a,c)]. Counterintuitively, in the $\mathcal{DMB}$ regime, for a lower laser power, each eigenvalue follows an enclosed path, beginning and ending at the same point; while for a higher laser power, both eigenvalues follow open trajectories, each of which ends at the starting point of the other, meaning the emergence of the EP owing to breaking the dark mode [see Figs. S2(b,d)]. By adjusting Δ and P, an EP (marked by the yellow star), where the eigenstates coalesce, appears when the system operates in the $\mathcal{DMB}$ regime, while not in the $\mathcal{DMN}$ regime.

D. Inactivation and activation of topological operations

In this section, we show in detail inactivation and activation of topological operations via dark-mode engineering. Specifically, when the system operates in either the symmetrical or asymmetrical optomechanical-coupling case, we display both vibrational resonance frequencies and decay rates versus a narrow range of the laser power P in both the $\mathcal{DMN}$ and $\mathcal{DMB}$ regimes, as shown in Fig. S3. In the $\mathcal{DMN}$ regime, only the bright mode evolves with P, while the dark mode remains invariant irrespective of the adjustment of system parameters, resulting in a completely deactivation of both the EP and topological operations [Fig. S3(a)]. It enables a complete blockade of the mode conversion and phonon transfer between the dark and

bright modes. However, in the $\mathcal{DMB}$ regime, both the bright and dark modes evolve simultaneously with P, which leads to the emergence of the characteristic features of the EP, enabling the activation of the EP and topological operations [Fig. S3(b)]. This offers, in general, an exciting opportunity of the revival of the mode conversion and phonon transfer between dark and bright modes.

Specifically, the eigenstates coalesce at a specific value of the control parameters, and in the vicinity of this point, they display a structure analogous to the Riemann surfaces of the complex square-root function. When executing a closed-loop path by adiabatically varying P and Δ, the generating smooth evolution on the eigenvalue manifold returns to its starting point only if the EP is not enclosed by the loop. In contrast, encircling the EP in a closed-loop trajectory induces a counterintuitive path starting on one sheet but ending on the other, giving rise to TPT. Our study sheds new light on the synergy of the dark-mode engineering and topological operations, offers an unconventional tool for tasks that cannot be executed by conventional topological mechanisms, and benefits for implementing dark-mode-free topological physics.

E. Eigenvalue distributions around an exceptional point

In this section, the eigenvalue distributions around an EP for different laser powers are shown in detail. In addition, we present in detail the transient behaviors of the studied systems in parameter spaces.

First, a detailed depiction of eigenvalue distributions around the EP is exhibited with the increasing of the laser powers. Physically, the imaginary and real parts of the complex eigenvalues of the two phonon modes are the mechanical linewidths $\gamma_{\pm}(\Delta, P) = -2\mathrm{Im}(\lambda_{\pm})$ and the mechanical resonance frequencies $\omega_{\pm}(\Delta, P) = \mathrm{Re}(\lambda_{\pm})$, respectively. We highlight that the manipulation of the optomechanical devices can be realized by a separate laser, which the driving detuning Δ and driving power P are set by an acousto-optic modulator. One can measure the mechanical spectra that is plotted as functions of the driving detuning Δ and the driving power P. As a result, we can accurately find the EP in the physical system. In particular, by driving the vibrations and monitoring their response via a heterodyne signal, these mechanical spectra can be easily acquired. One can fit each spectrum to tune the two mechanical resonance frequencies, $\omega_{\pm}(\Delta, P)$ and the two mechanical decay rates $\gamma_{\pm}(\Delta, P)$. Here we emphasize that the subscripts "±" refer to the phonon normal modes, when applying the driving field into the investigated physical system.

(i) In the symmetrical optomechanical coupling case (i.e., $g_2 = g_1$), we show in the $\mathcal{DMB}$ regime that when $P < P_{\mathrm{EP}} \approx 344.5$ uW, the eigenfrequencies exhibit an identical imaginary part and two different real parts, which, respectively, indicate that the system possesses an identical mechanical linewidth and two different mechanical resonance frequencies [see the left-hand sides of Figs. S3(d) and S3(b)]. This refers to the $\mathcal{PT}$-symmetric regime. When $P > P_{\mathrm{EP}} \approx 344.5$ uW, the eigenfrequencies have two different imaginary parts and an identical real part, which means the appearance of two different mechanical linewidths and an identical mechanical resonance frequency, respectively, as shown on the right-hand sides of Figs. S3(d) and S3(b). This corresponds to the broken-$\mathcal{PT}$-symmetric regime. Clearly, the phase transition of the system is presented around the border point $P = P_{\mathrm{EP}} \approx 344.5$ uW, indicating the emergence of an EP [see the yellow stars in Figs. S3(d) and S3(b)].

(ii) In the asymmetrical optomechanical coupling case (i.e., $g_2 = 2.76g_1$), we find in the $\mathcal{DMB}$ regime that when $P < P_{\mathrm{EP}} \approx 108$ uW or $P > P_{\mathrm{EP}} \approx 108$ uW, the eigenfrequencies always exhibit two different real parts and two different imaginary parts, corresponding to two different mechanical resonance frequencies and two different mechanical linewidths, respectively [see Figs. S3(f) and S3(h)]. In particular, the phase transition of the system is presented around the border point $P = P_{\mathrm{EP}} \approx 108$ uW, corresponding to an EP [see the yellow discs in Figs. S3(f) and S3(h)].

III. DARK-MODE-ENGINEERED TOPOLOGICAL PHONONICS

In this section, we define a topological-phonon-transfer efficiency to quantify the energy transfer between the two motional normal modes, and show in detail topological phonon blockade and its transfer via dark-mode engineering, and dark-mode-controlled nonreciprocal topological dynamics.

A. Efficiency of topological phonon transfer

The projection onto the instantaneous eigenbasis is necessary to see the state evolution during the applied perturbations. Allow $\vec{v}_{\pm}(t)$ to serve as the instantaneous eigenvectors of $\mathcal{H}_{\mathrm{eff}}$. Whenever necessary, the solution $\vec{b}(t) = \Big(b_1(t),\ b_2(t)\Big)^T$ can be written as a projection based on this basis,

$$\vec{b}(t) = \mathcal{B}_{-}(t)\vec{v}_{-}(t) + \mathcal{B}_{+}(t)\vec{v}_{+}(t). \tag{S62}$$

If the perturbation is slow compared to the energy gap ($\lambda_+ - \lambda_-$), one naive and unjustified approach to thinking about this system would be to assume that adiabaticity (in the sense of smooth evolution along the eigenvalue surface) would occur as long as the perturbation is slow. That is, if we were to prepare $\mathcal{B}_-(0) = 1$ and $\mathcal{B}_+(0) = 0$, then for all times t, $\mathcal{B}_-(t) = 1$ remains the dominant projection. We can use standard computational techniques to numerically integrate the linear differential equations to see if this happens. The calculation provides a complete solution for the system's time-dependent nature, $\vec{b}(t)$. It is worth pointing out that this result is based on the differential equation, not the eigenbasis. (i.e. $b_{1,2}(t)$ not $\mathcal{B}_\pm(t)$). A change of the basis defined by a matrix of instantaneous eigenvectors is necessary to find the projection into the instantaneous eigenbasis,

$$\begin{pmatrix} \mathcal{B}_+(t) \\ \mathcal{B}_-(t) \end{pmatrix} = \mathbf{N}(t) \begin{pmatrix} b_1(t) \\ b_2(t) \end{pmatrix}. \tag{S63}$$

where

$$\mathbf{N}(t) = \left[\begin{pmatrix} \vec{v}_+(t) & \vec{v}_-(t) \end{pmatrix}^T \right]^{-1}. \tag{S64}$$

We have already mentioned that this energy transfer is a result of an adiabatic-like process, and should be influenced by the geometry of the loop, in relation to the topology of the eigenvalue manifolds. A metric for quantifying energy transfer would be beneficial, in order to systematically characterize this behavior. Essentially, if we initialize the system into a particular mode, i.e., $\mathcal{B}_\pm(t = 0) = 1$, we would like to know the amplitude of the other mode at the end of the loop, i.e., $\mathcal{B}_\mp(t) = 1$. Normalizing the total energy at the end of the loop is necessary, owing to the growth/decay of the overall system energy. To quantify the energy transfer from one motional normal mode ($\mathcal{B}_-$) to the other ($\mathcal{B}_+$), we define an efficiency of topological phonon transfer:

$$\mathbf{F}_+ = \frac{|\mathcal{B}_+(\tau)|^2}{|\mathcal{B}_+(\tau)|^2 + |\mathcal{B}_-(\tau)|^2}, \tag{S65}$$

denoting the fraction of the remaining energy in the $\mathcal{B}_+$ mode after executing the control loops. Analogously, we can define $\mathbf{F}_- = 1 - \mathbf{F}_+$. Note that before performing all the control loops, the definition of $\mathbf{F}_+$ needs to satisfy the condition that all energy remains in $\mathcal{B}_-$. Specifically, we see from Eq. (S65) that

$$\mathbf{F}_+ \to 0 \tag{S66}$$

indicates that no energy transfer occurs from the vibrational mode $\mathcal{B}_-$ to $\mathcal{B}_+$; while a *perfect* energy transfer happens from $\mathcal{B}_-$ to $\mathcal{B}_+$ when

$$\mathbf{F}_+ \to 1. \tag{S67}$$

That is before the adiabatic control loop, 100% of the energy is concealed in the $\mathcal{B}_-$ mode, whereas after the adiabatic loop, 100% of the remaining energy is in the $\mathcal{B}_+$ mode. We here should emphasize that our analysis and numerical simulations were all made assuming injecting the initial drive to the motional normal mode $\mathcal{B}_-$, and subsequently, performing a control loop only in the counter-clockwise direction. In this case, the adiabatic paths enclosing the EP correspond to the less-damped eigenmode for the majority of the control loop. On the contrary, executing clockwise the same control loop leads to an adiabatic path, which corresponds primarily to the more-damped eigenmode. Next, we study in detail the topological phonon blockade and its transfer via dark-mode control.

B. Topological phonon blockade and its transfer by engineering dark modes

The dark mode naturally decoupled from the system results in a complete blockade of both the mode conversion and phonon transfer between the dark and bright modes. Surprisingly, this dark mode can be controlled at will by simply employing synthetic magnetism (i.e., $\xi \neq 0$ and $\Theta \neq n\pi$). Note that this synthetic magnetism can be achieved at will using a phase-dependent loop-coupled configuration, which results in an effective synthetic gauge field [S13–S21], inducing a path interference between two phonon-transfer channels. Physically, the dark mode can be flexibly engineered just by tuning the synthetic magnetism in our phase-dependent loop-coupled optomechanical system.

We reveal that executing a topological operation in the $\mathcal{DMN}$ regime yields the TPB between the dark and bright modes (see blue dashed lines in Fig. S4); whereas performing it in the $\mathcal{DMB}$ regime gives rise to the TPT (see red curves in Fig. S4). This enables a versatile yet unique topological physics and provides an exciting possibility of bridging the TPB and TPT at will, as shown in Fig. S4, which is otherwise unattainable in previously established demonstrations [S1, S2, S40–S52]. Unlike previous schemes, where both EPs and topological operators are entirely malfunctioning in the presence of dark modes [S1, S2, S40–S52], our approach is entirely immune to this detrimental inactivation effect. In a broader view, our study sheds new light on

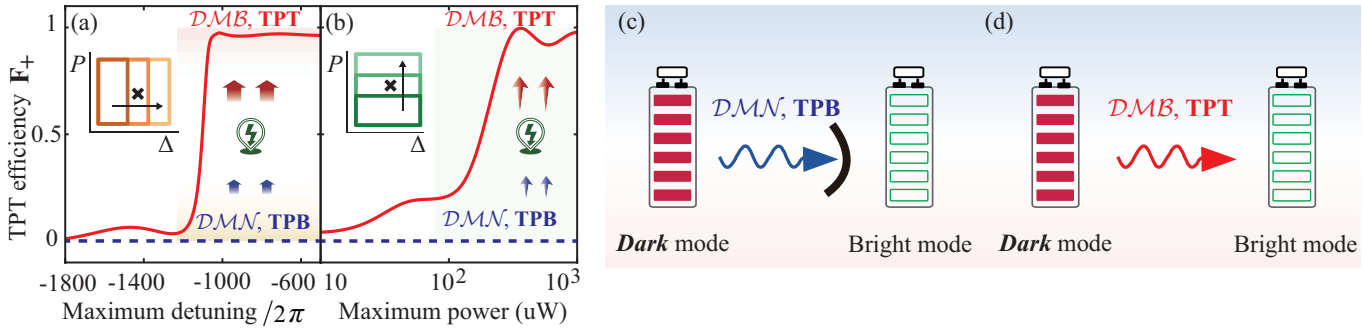

FIG. S4: (a,b) Efficiency $\mathbf{F}_+$ of TPT from the dark to bright modes versus the maximum driving: (a) detuning $\Delta_{\rm Max}$ and (b) power $P_{\rm Max}$, by executing a closed control loop. Two insets show how the loops vary along the horizontal axis of each panel, and the black crosses indicate the location of the EP. (c,d) Imposing topological operations in (c) the $\mathcal{DMN}$ ($g_2 = g_1$, $\xi/\omega_1 = 5\times10^{-4}$, and $\Theta = 0$) and (d) $\mathcal{DMB}$ ($g_2 = 2.76g_1$, $\xi/\omega_1 = 5\times10^{-4}$, and $\Theta/\pi = 1/9$) regimes yields TPB and TPT, respectively.

the combination of the dark-mode engineering, topological operations, and quantum networks, and offers an exciting prospect of revealing a unique topology with immunity against dark modes.

Specifically, the TPT efficiency $\mathbf{F}_+$ is plotted versus $\Delta_{\rm Max}$ and $P_{\rm Max}$ in both the $\mathcal{DMN}$ and $\mathcal{DMB}$ regimes, as shown in Figs. S4(a,b). We reveal that in the $\mathcal{DMN}$ regime, TPB occurs ($\mathbf{F}_+ = 0$, blue dashed lines); while in the $\mathcal{DMB}$ regime, an excellent TPT emerges ($\mathbf{F}_+ = 1$, red solid curves). Specifically, in the $\mathcal{DMN}$ regime, thermal phonons concealed in the dark mode cannot be transferred to the bright mode regardless of the tuning of the system parameters, giving rise to TPB [see Fig. S4(c)]. In stark contrast to this, in the $\mathcal{DMB}$ regime, an efficient extraction of thermal phonons stored in the dark mode to the bright mode is achieved, enabling the TPT [Fig. S4(d)]. These findings demonstrate that simply utilizing the dark-mode control enabled by synthetic magnetism establishes not only an extremely flexible switch between TPB and TPT, but also provides a possibility of immunizing all topological quantum resources against various dark-mode disturbances in practical devices.

Physically, in conventional schemes (i.e., without the synthetic magnetism), all topological behaviors are inherently fragile to dark modes decoupled from the system, leading to a complete malfunction of both EPs and topological operations [S1, S2]. However, by employing the synthetic magnetism, all topological responses are immune to these dark modes, resulting in the function of topological operations. Our approach offers a new way enabling practical dark-mode-sensitive setups to be ideal, beneficial for achieving dark-mode-immune topological resources.

$$\begin{cases} \text{Tuning } \Theta \Rightarrow \text{Switching between the } \mathcal{DMN} \text{ and } \mathcal{DMB} \text{ regimes;} \\ \mathcal{DMN} \Rightarrow \text{Inactivation of topological operations} \Rightarrow \text{TPB;} \\ \mathcal{DMB} \Rightarrow \text{Activation of topological operations} \Rightarrow \text{TPT.} \end{cases} \tag{S68}$$

C. Dark-mode-engineered nonreciprocal topological dynamics

To study the dependence of one-way topological dynamics on the dark-mode engineering, we display the TPT efficiency versus the duration τ of the closed control loops, when the system operates in the $\mathcal{DMN}$ and $\mathcal{DMB}$ regimes, as shown in Fig. S5. In the $\mathcal{DMN}$ regime, TPB always happens ($\mathbf{F}_+ = 0$) no matter how to execute the EP-enclosing control loops in parameter spaces (see lower solid horizontal lines). In the $\mathcal{DMB}$ regime, by rapidly winding around the EP (i.e., $\tau \to 0$), TPB (i.e., $\mathbf{F}_+ \to 0$) is observed; while with adiabatically encircling this EP (i.e., $\tau \gg 1$ ms [S1]), an excellent TPT appears (i.e., $\mathbf{F}_+ \to 1$). These findings demonstrate that a vanishing TPT, corresponding to the emergence of TPB, is resulting from either the dark mode for the $\mathcal{DMN}$ regime or a rapid encirclement of the EP for the $\mathcal{DMB}$ regime.

By adiabatically winding around the EP, the TPT limiting behavior is contingent upon both the direction of the loop and the mode initially excited. For example, by executing a clockwise (counterclockwise) loop, the blue (red) data represent conventional adiabaticity ($\mathbf{F}_+ \to 1$ when increasing τ), while the red (blue) data show an opposite behavior ($\mathbf{F}_+ \to 0$ as increasing τ). These results clearly elucidate the *nonreciprocity* of each topological operation for an anticlockwise or clockwise control loop enclosing an EP.

IV. SCALABLE NETWORK-BASED TOPOLOGICAL PHONON TRANSFER VIA SYNTHETIC MAGNETISM

In this section, the established dark-mode-engineering mechanism, induced by synthetic magnetism, is generalized to generate the TPT networks in optomechanical networks, consisting of a single photon mode optomechanically coupled to N phonon

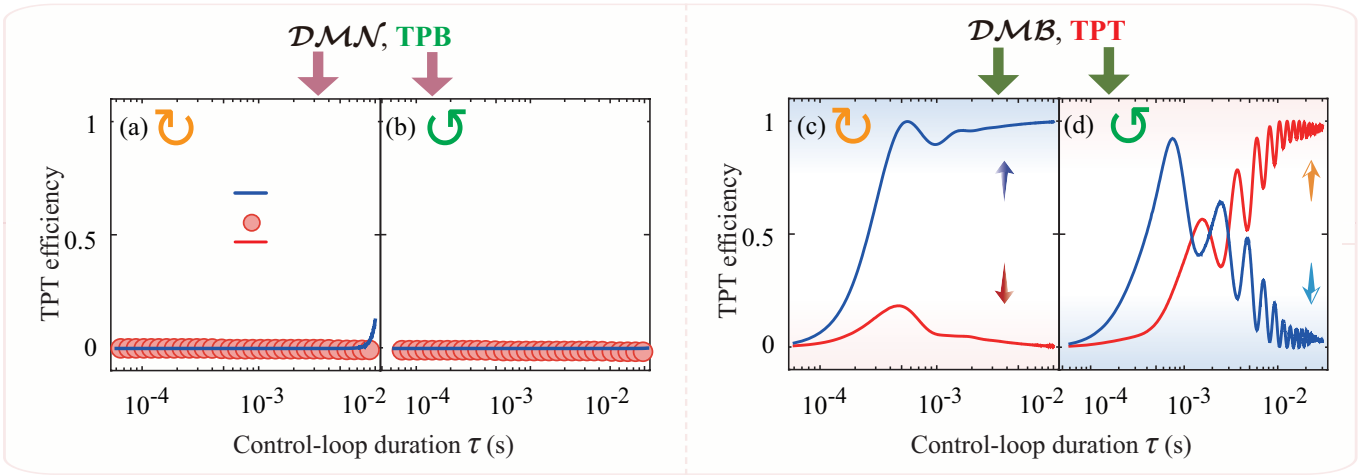

FIG. S5: Efficiency of TPT versus the duration τ of a closed control loop, in the $\mathcal{DMN}$ ($g_2 = g_1$, $\xi/\omega_1 = 5\times10^{-4}$, and $\Theta = 0$) and $\mathcal{DMB}$ ($g_2 = 2.76g_1$, $\xi/\omega_1 = 5\times10^{-4}$, and $\Theta/\pi = 1/9$) regimes. The control-loop shape enclosing an EP is the same for all data series, and this EP is encircled in (a) the clockwise and (b) counterclockwise directions. Blue or red curves correspond to the data where the bright or dark mode is initially excited, respectively.

modes.

A. Dark-mode engineering in quantum optomechanical networks

In this section, we elucidate the dark modes in an optomechanical network consisting of N ($N \geq 3$) phonon modes optomechanically coupled to a common photon mode, and the nearest-neighboring phonon modes coupled to each other through the phase-dependent phonon-hopping interactions. For convenience, we focus on the case of no interaction between the last and the first phonon modes. Then, the optomechanical-network Hamiltonian reads

$$\mathcal{H} = \omega_c a^\dagger a + \sum_{j=1}^{N}[\omega_j b_j^\dagger b_j + g_j a^\dagger a(b_j^\dagger + b_j)] + \sum_{j=1}^{N-1}\xi_j(e^{i\Theta_j}b_j^\dagger b_{j+1} + e^{-i\Theta_j}b_{j+1}^\dagger b_j) + i\sqrt{\kappa_{\rm in}}\epsilon_{\rm in}(a^\dagger e^{-i\omega_l t} - \text{H.c.}). \tag{S69}$$

The phase-dependent phonon-hopping interactions between the nearest-neighboring phonon modes are employed with coupling strengths ξ_j and modulation phases Θ_j. As a result, the synthetic gauge fields, which is used to manipulate the dark mode, can be induced by using a phase-dependent loop-coupled setup that is made up of the g_j and ξ_j terms.

Now, the research procedure, which is similar to that used in the two-phonon-mode case (see Sec. I A), is applied to infer a linearized optomechanical Hamiltonian, which governs the evolution of quantum fluctuations. Specifically, this is achieved by applying a linearization procedure and expanding all operators $o \in\{a,\, b_j,\, a^\dagger,\, b_j^\dagger\}$ as sums of their classical averages and quantum fluctuations, i.e., $o = \bar{o} + \delta o$. Subsequently, the linearized optomechanical Hamiltonian for quantum fluctuations, in the N-phonon-mode case, takes the following form:

$$\mathcal{H}_I = -\Delta\delta a^\dagger\delta a + \omega_j\textstyle\sum_{j=1}^{N}\delta b_j^\dagger\delta b_j + \sum_{j=1}^{N}G_j(\delta a^\dagger\delta b_j + \delta b_j^\dagger\delta a) + \mathcal{H}_{\rm phi}, \tag{S70}$$

where $\Delta \approx \omega_L - \omega_c$ is the driving detuning after the linearization procedure, and $G_j = g_j\bar{a}$ is the linearized optomechanical-coupling strength between the jth phonon mode and the photon mode. The last term in Eq. (S70) is given by

$$\mathcal{H}_{\rm phi} = \textstyle\sum_{j=1}^{N-1}\mathcal{H}_j, \tag{S71}$$

where the subscript "phi" stands for the phonon-hopping interaction of the Hamiltonian, and

$$\mathcal{H}_j = \xi_j(e^{-i\Theta_j}\delta b_j\delta b_{j+1}^\dagger + e^{i\Theta_j}\delta b_{j+1}\delta b_j^\dagger), \tag{S72}$$

describes the phonon-hopping interaction between the jth and $(j+1)$th phonon modes.

To study the dark modes in the N-phonon-mode optomechanical system, we first consider the case where the phase-dependent phonon-hopping interaction is absent, i.e., $\mathcal{H}_{\rm phi} = 0$. For convenience, we assume that all the phonon modes have the same resonance frequency (i.e., $\omega_j = \omega_m$) and optomechanical-coupling strength (i.e., $G_j = G$).

In this case, there exists a single bright mode

$$\mathcal{B} = \frac{1}{\sqrt{N}} \sum_{j=1}^{N} \delta b_j, \quad \textit{bright} \text{ mode}, \tag{S73}$$

and $N-1$ dark modes which are completely decoupled from both the bright mode and the photon mode.

To control all the dark modes in the N-phonon-mode optomechanical system, we employ phase-dependent phonon-hopping interactions $\mathcal{H}_{\rm phi}$, which in combination with optomechanical couplings are utilized for forming a phase-dependent loop-coupled configuration, resulting in the synthetic magnetism. Without loss of generality, we assume that all the coupling strengths of the phonon-hopping couplings are the same, i.e., $\xi_j = \xi$. Thus, we diagonalize the Hamiltonian of these coupled phonon modes to obtain the phonon-hopping terms, i.e.,

$$\mathcal{H}_{\rm pht} = \omega_m \sum_{j=1}^{N} \delta b_j^{\dagger} \delta b_j + \xi \sum_{j=1}^{N-1} (e^{-i\Theta_j} \delta b_j \delta b_{j+1}^{\dagger} + e^{i\Theta_j} \delta b_{j+1} \delta b_j^{\dagger}) = \sum_{k=1}^{N} \Omega_k B_k^{\dagger} B_k, \tag{S74}$$

where the subscript "pht" depicts the phonon-hopping terms of the Hamiltonian, and B_k is the kth phonon normal mode with its resonance frequency defined as

$$\Omega_k = \omega_m + 2\xi \cos\left(\frac{k\pi}{N+1}\right), \qquad k = 1, 2, 3, \cdots, N. \tag{S75}$$

Subsequently, the phonon modes δb_j and the normal modes B_k can be related by

$$\delta b_j = \begin{cases} \frac{1}{A} \sum_{k=1}^{N} \sin\left(\frac{k\pi}{N+1}\right) B_k, & j = 1, \\ \frac{1}{A} e^{-i\sum_{\nu=1}^{j-1}\Theta_\nu} \sum_{k=1}^{N} \sin\left(\frac{jk\pi}{N+1}\right) B_k, & j \geq 2, \end{cases} \tag{S76}$$

where $A = \sqrt{(N+1)/2}$. Then, with these phonon normal modes, we can rewrite the Hamiltonian in Eq. (S70) as

$$\mathcal{H}_I = \Delta \delta a^{\dagger} \delta a + \textstyle\sum_{k=1}^{N} \Omega_k B_k^{\dagger} B_k + \mathcal{H}_{\rm om}, \tag{S77}$$

with $H_{\rm om}$ being the optomechanical-coupling Hamiltonian, which reads

$$\mathcal{H}_{\rm om} = \sum_{k=1}^{N} \left\{ \frac{G}{A} \left[\sin\left(\frac{k\pi}{N+1}\right) + \sum_{j=2}^{N} e^{i\sum_{\nu=1}^{j-1}\Theta_\nu} \sin\left(\frac{jk\pi}{N+1}\right) \right] a B_k^{\dagger} + \text{H.c.} \right\}. \tag{S78}$$

When $N \geq 3$, the coupling Hamiltonian $\mathcal{H}_{\rm ck}$ between the cavity-field mode a and the kth normal mode B_k can be expressed based on Eq. (S78) as

$$\mathcal{H}_{\rm ck} = G_{\rm eff}^{(k)}(N) a B_k^{\dagger} + \text{H.c.}, \tag{S79}$$

where the effective coupling strength $G_{\rm eff}^{(k)}(N)$ shown in Eq. (S79), between the photon mode a and the kth normal mode B_k, is defined as

$$G_{\rm eff}^{(k)}(N) = \frac{G}{A} \left[\sin\left(\frac{k\pi}{N+1}\right) + \sum_{j=2}^{N} e^{i\sum_{\nu=1}^{j-1}\Theta_\nu} \sin\left(\frac{jk\pi}{N+1}\right) \right]. \tag{S80}$$

Obviously, we see from Eq. (S80) that the total effect of these modulation phases in the optomechanical interactions is simply governed by the sum $\sum_{\nu=1}^{j-1}\Theta_\nu$. Consequently, a single modulation phase can be applied to achieve dark-mode engineering. For convenience, the case of $\Theta_j = 0$ for $j = 2, \cdots, N-1$ has been considered in the following discussions, and subsequently,

Eq. (S80) can be easily divided into the following four forms:

$$G_{\rm eff}^{(k=\rm odd)}(N=\rm odd) = \frac{G}{A}\Big[(1+e^{i\Theta_1})\sin\left(\frac{k\pi}{N+1}\right)+2e^{i\Theta_1}\sin\left(\frac{2k\pi}{N+1}\right) + 2e^{i\Theta_1}\sin\left(\frac{3k\pi}{N+1}\right)+\cdots+2e^{i\Theta_1}\sin\left(\frac{(N-1)k\pi}{2(N+1)}\right) + e^{i\Theta_1}\sin\left(\frac{k\pi}{2}\right)\Big], \tag{S81}$$

$$G_{\rm eff}^{(k=\rm odd)}(N=\rm even) = \frac{G}{A}\Big[(1+e^{i\Theta_1})\sin\left(\frac{k\pi}{N+1}\right)+2e^{i\Theta_1}\sin\left(\frac{2k\pi}{N+1}\right) + 2e^{i\Theta_1}\sin\left(\frac{3k\pi}{N+1}\right)+\cdots+2e^{i\Theta_1}\sin\left(\frac{Nk\pi}{2(N+1)}\right)\Big], \tag{S82}$$

$$G_{\rm eff}^{(k=\rm even)}(N=\rm odd) = \frac{G}{A}\left(1-e^{i\Theta_1}\right)\sin\left(\frac{k\pi}{N+1}\right), \tag{S83}$$

$$G_{\rm eff}^{(k=\rm even)}(N=\rm even) = G_{\rm eff}^{(k=\rm even)}(N=\rm odd). \tag{S84}$$

According to Eqs. (S81)- (S84), it shows that for an odd number k, the effective coupling strength between the photon mode a and the kth normal mode B_k is nonzero, i.e.,

$$G_{\rm eff}^{(k=\rm odd)}(N) \neq 0. \tag{S85}$$

However, we see that for an even number k, the effective coupling strength is expressed as

$$G_{\rm eff}^{(k=\rm even)}(N) = \frac{G}{A}\left(1-e^{i\Theta_1}\right)\sin\left(\frac{k\pi}{N+1}\right). \tag{S86}$$

Clearly, Eqs. (S79) and (S86) imply that when

$$\Theta_1 = 2n\pi, \tag{S87}$$

the strength of the effective coupling, between an even normal mode $B_{k=\rm even}$ and the photon mode a, is equal to zero, i.e.,

$$G_{\rm eff}^{(k=\rm even)}(N) = 0. \tag{S88}$$

In this case, all the even normal modes are decoupled from the photon mode and the system. Therefore, the TPT cannot happen because of the emergence of the dark modes. As a result, the breaking of all $N-1$ dark modes in optomechanical networks can be flexibly realized by simply tuning the modulation phase

$$\Theta_1 \neq 2n\pi. \tag{S89}$$

Our findings establish a versatile platform for an on-demand switching of quantum optomechanical networks between the $\mathcal{DMN}$ and $\mathcal{DMB}$ regimes, unlocking new possibilities for dynamic control in quantum networks.

Here, we highlight the fundamental significance and broad implications of our dark-mode engineering approach, which resolves a persistent and critical challenge in topological phononics. Notably, two seminal back-to-back studies [S1, S2] implicitly revealed a fundamental constraint in the field of topological phononics: dark modes inherently suppress topological dynamics, thereby impeding both mode conversion and phonon transport. Our work directly addresses this limitation, offering a transformative solution to unlock previously inaccessible topological phenomena.

While previous studies have primarily sought to circumvent dark modes [S1, S2], our work directly confronts and addresses the fundamental challenge posed by dark-mode contaminations. By engineering phase-dependent phonon-hopping interactions, we selectively activate dark modes to enable topological phonon transport and topological mode switching. Crucially, unlike existing approaches [S1], which rely on non-degenerate mechanical resonators to achieve topological encircling around an EP, we demonstrate that even degenerate mechanical resonators can exhibit analogous topological behavior. This finding is both counterintuitive and unprecedented, representing a significant conceptual advance in topological phonics.

In particular, the proposed dark-mode engineering mechanism demonstrates substantial conceptual originality, bridging quantum optomechanics and topological physics. A recent experiment [S53] had emphasized that dark modes decoupled from the system defy quantum ground-state preparation, restricting cooling to the bright mode alone. Leveraging this framework, we pioneer the exploitation of dark-bright mode engineering to uncover topological phenomena, enabling both TPT and TPB between dark and bright modes. This breakthrough establishes a previously unexplored paradigm for topological control in quantum optomechanical systems.

B. Scalable network-based topological phonon transfer

In this section, we further generalize our dark-mode-engineering method to generate the scalable network-based TPT and TPB in quantum optomechanical network, where an photon mode couples to N phonon modes via radiation-pressure interactions, and the nearest-neighbor phonon modes are coupled to each other through the phase-dependent phonon-exchange couplings.

Note that in Sec. IV A, we have demonstrated in detail that, when synthetic magnetism is absent, there only a single bright mode coupled to the system is induced and $N-1$ dark modes are decoupled from the optical mode, and that owing to synthetic magnetism, all the dark modes can be engineered by tuning the modulation phase. Specifically, we reveal that in the absence of synthetic magnetism, there is only a single bright mode and $N-1$ dark modes. Surprisingly, synthetic gauge fields, induced by the phase-dependent loop-coupled quantum networks, can lead to a simultaneous breaking of all $N-1$ dark modes, offering an exciting opportunity of switching a quantum network between the $\mathcal{DMN}$ and $\mathcal{DMB}$ regimes. Therefore, thermal phonons from the dark to bright modes are blockaded in the $\mathcal{DMN}$ regime, while transferred in the $\mathcal{DMB}$ regime, making the TPT between the dark and bright modes feasible. These findings mean that the scalable network-based TPT, which is immune to dark modes, can be achieved just by applying the dark-mode engineering to quantum optomechanical networks.

In this work, we have demonstrated a versatile switch between TPB and TPT arising from a general dark-mode engineering, without which it vanishes. Note that our study differs from what is known in previously established demonstrations, mainly because we are focused on overcoming the challenging from dark-mode contamination in the topological response, but not on deliberately circumventing it. Our work provides a general approach to engineer and protect topological resources from dark modes, and maps a new perspective on constructing an unconventionally nonreciprocal topology and topological quantum networks with immunity against dark modes.

V. QUANTUM COLLECTIVE MOTION USING DARK-MODE ENGINEERING

The proposed dark-mode engineering mechanism has a broad applicability and relevance, because it could introduce a versatile strategy with wide-ranging implications. Specifically, the framework developed here can be broadly applied to control collective quantum motion in macroscopic mechanical systems. As highlighted in Ref. [S53], the quantum control of collective phonon modes in large-scale mechanical resonators represents an emerging research frontier. Our method for engineering nonreciprocal and topological phonon transfer via dark-mode manipulation contributes a powerful and widely applicable tool for this growing field.

Specifically, this breakthrough experiment [S53] highlights a key limitation in observing quantum collective motion in macroscopic mechanical resonators: Only a single bright mode, coupled to the system, can be cooled to its quantum ground state, while all $N-1$ dark modes remain entirely decoupled from the system. This inherent decoupling renders the dark modes inaccessible to conventional quantum control and ground-state preparation. Building on this pioneering work [S53], our study fundamentally overcomes this constraint by introducing a mechanism that enables simultaneous ground-state preparation of both bright and dark modes. By simply activating synthetic magnetism, our scheme unlocks the full quantum potential of collective phononic dynamics. In doing so, it establishes a new paradigm in quantum optomechanics, which is no longer bound by the limitations imposed by dark modes.

We show that in the $\mathcal{DMN}$ regime, all dark modes remain uncooled; whereas in the $\mathcal{DMB}$ regime, they are simultaneously cooled to their quantum ground states. These counterintuitive phenomena arise from the underlying physical mechanism: dark modes are naturally decoupled from the system and then, thermal noise trapped in dark modes cannot be extracted through sideband cooling [S54–S57], making the quantum ground-state preparation of these dark modes unattainable [S53]. In contrast, upon transitioning into the $\mathcal{DMB}$ regime, simultaneous quantum ground-state preparation of both dark and bright modes becomes achievable near the red-sideband resonance. These findings demonstrate that the proposed dark-mode engineering offers flexible control and effective protection of fragile collective quantum ground states.

In the following, we will elucidate in detail how dark-mode manipulation overcomes this outstanding challenge imposed by dark modes, enabling simultaneous quantum ground-state preparation of both dark and bright modes.

A. Dark–bright mode engineering

In Sec. IV A, we have detailedly demonstrated how to control both the dark and bright modes in quantum optomechanical networks, consisting of N mechanical modes coupled to a shared cavity-field mode. Evidently, we see from Eq. (S86) that when $\Theta_1 = 2n\pi$, the emergence of dark modes that completely decouple from the system gives rise to the $\mathcal{DMN}$ regime. Surprisingly, however, by simply tuning $\Theta_1 \neq 2n\pi$, all dark modes can acquire finite effective couplings to the system, thereby transitioning into the $\mathcal{DMB}$ regime. Consequently, while achieving the quantum ground state for all dark modes is inherently unattainable in the $\mathcal{DMN}$ regime, it is, counterintuitively, rendered feasible in the $\mathcal{DMB}$ regime.

In the groundbreaking experimental work [S53], it shows that the coupling of N phonon modes to a shared photon mode results in a single bright mode coupled to the system and $N-1$ dark modes are decoupled from this system. Consequently, although the quantum ground state can be prepared only for the bright mode, it remains intrinsically unattainable for all dark modes [S53]. Building upon this pioneering work [S53], the proposed dark-mode engineering method can directly address this outstanding challenge posed by dark modes, introducing a novel paradigm for the quantum ground-state cooling of both the dark and bright modes.

Below, we establish a quantitative framework for quantum collective ground-state cooling by deriving exact expressions for the final phonon occupancies in both dark and bright modes.

B. Occupations of dark and bright modes

By utilizing the covariance matrix representation in the basis of mechanical modes, we can systematically quantify the phonon occupation in all dark and bright modes. Given that the initial state is Gaussian, the Gaussian nature of the state is preserved throughout its evolution. As a result, the covariance matrix provides a complete description of the system and, in the vibrational-mode basis, takes the form [S53]

$$\mathrm{Cov} = \begin{pmatrix} \left\langle \delta b_1^\dagger \delta b_1 \right\rangle & \left\langle \delta b_1^\dagger \delta b_2 \right\rangle & \cdots & \left\langle \delta b_1^\dagger \delta b_N \right\rangle \\ \left\langle \delta b_2^\dagger \delta b_1 \right\rangle & \left\langle \delta b_2^\dagger \delta b_2 \right\rangle & \cdots & \left\langle \delta b_2^\dagger \delta b_N \right\rangle \\ \vdots & \vdots & \ddots & \vdots \\ \left\langle \delta b_N^\dagger \delta b_1 \right\rangle & \left\langle \delta b_N^\dagger \delta b_2 \right\rangle & \cdots & \left\langle \delta b_N^\dagger \delta b_N \right\rangle \end{pmatrix}, \tag{S90}$$

where

$$\left\langle \delta b_i^\dagger \delta b_j \right\rangle = \frac{1}{2\pi} \int_{-\infty}^{+\infty} S_{b_i^\dagger b_j}(\omega)\, d\omega. \tag{S91}$$

The occupations of the dark and bright modes can be directly determined by diagonalizing the covariance matrix Eq. (S90). The eigenvalues of Eq. (S90) encapsulate the occupations of these collective modes: the lowest eigenvalue corresponds to the phonon numbers in a single bright mode (i.e., $n_{\mathcal{B}}$), while the remaining $N-1$ eigenvalues represent the occupations of $N-1$ dark modes (i.e., $n_{\mathcal{D}_l}$), respectively.

Given the presence of $N-1$ dark modes, we define the mean phonon number of these dark modes as

$$n_{\mathcal{D}} = \frac{1}{N-1} \sum_{l=1}^{N-1} n_{\mathcal{D}_l}, \tag{S92}$$

which explicitly reveals that the condition $n_{\mathcal{D}} < 1$ signifies simultaneous preparation of all dark modes in their quantum ground states.

C. Quantum collective ground-state preparation of both dark and bright modes

The strategic engineering of dark modes provides a viable pathway for realizing and protecting fragile quantum collective motion from various disturbances associated with dark modes in practical devices. Furthermore, it facilitates the implementation of noise-free quantum optomechanical networks.

We demonstrate that in the $\mathcal{DMN}$ regime, all dark modes persist in an uncooled state ($n_{\mathcal{D}} = 10^3$), whereas in the $\mathcal{DMB}$ regime, they are efficiently cooled to their quantum motional ground states ($n_{\mathcal{D}} < 1$). The underlying mechanism arises from the intrinsic decoupling of dark modes in the $\mathcal{DMN}$ regime, which suppresses thermal phonon extraction via sideband cooling [S54–S57], thereby precluding their quantum ground-state cooling.

In stark contrast to this, when the system operates in the $\mathcal{DMB}$ regime, all dark and bright modes can be simultaneously driven into their quantum ground states near the red-sideband resonance, i.e., $\Delta \approx -\omega_m$. These findings highlight that the preparation of fragile quantum collective ground states can be not only flexibly engineered but also robustly protected through synthetic magnetism.

[S1] Xu, H., Mason, D., Jiang, L. & Harris, J. G. E. Topological energy transfer in an optomechanical system with exceptional points. Nature **537**, 80 (2016).

[S2] Doppler, J. *et al*. Dynamically encircling an exceptional point for asymmetric mode switching. Nature **537**, 76 (2016).

[S3] Kitagawa, T. *et al*. Observation of topologically protected bound states in photonic quantum walks. Nat. Commun. **3**, 882 (2012).

[S4] Malzard, S., Poli, C. & Schomerus, H. Topologically Protected Defect States in Open Photonic Systems with Non-Hermitian Charge-Conjugation and Parity-Time Symmetry. Phys. Rev. Lett. **115**, 200402 (2015).

[S5] Cardano, F. *et al*. Statistical moments of quantum-walk dynamics reveal topological quantum transitions. Nat. Commun. **7**, 11439 (2016).

[S6] Rechtsman, M. C. *et al*. Topological protection of photonic path entanglement, Optica **3**, 925 (2016).

[S7] Mittal, S., Orre, V. V. & Hafezi, M. Topologically robust transport of entangled photons in a 2D photonic system. Opt. Express **24**, 15631 (2016).

[S8] Gorlach, M. A. & Poddubny, A. N. Topological edge states of bound photon pairs. Phys. Rev. A **95**, 053866 (2017).

[S9] Barik, S. *et al*. A topological quantum optics interface. Science **359**, 666 (2018).

[S10] Blanco-Redondo, A. *et al*. Topological protection of biphoton states. Science **362**, 568 (2018).

[S11] Mittal, S., Goldschmidt, E. A. & Hafezi, M. A topological source of quantum light. Nature **561**, 502 (2018).

[S12] Mittal, S., Orre, V. V., Goldschmidt, E. A. & Hafezi, M. Tunable quantum interference using a topological source of indistinguishable photon pairs. Nat. Photonics **15**, 542 (2021).

[S13] Schmidt, M., Kessler, S., Peano, V., Painter, O. & Marquardt, F. Optomechanical creation of magnetic fields for photons on a lattice. Optica **2**, 635 (2015).

[S14] Shen, Z. *et al*. Experimental realization of optomechanically induced non-reciprocity. Nat. Photonics **10**, 657 (2016).

[S15] Ruesink, F., Miri, M.-A., Alù, A. & Verhagen, E. Nonreciprocity and magnetic-free isolation based on optomechanical interactions. Nat. Commun. **7**, 13662 (2016).

[S16] Fang, K. *et al*. Generalized non-reciprocity in an optomechanical circuit via synthetic magnetism and reservoir engineering. Nat. Phys. **13**, 465 (2017).

[S17] Bernier, N. R. *et al*. Nonreciprocal reconfigurable microwave optomechanical circuit. Nat. Commun. **8**, 604 (2017).

[S18] Shen, Z. *et al*. Reconfigurable optomechanical circulator and directional amplifier. Nat. Commun. **9**, 1797 (2018).

[S19] Ruesink, F., Mathew, J. P., Miri, M.-A., Alù, A. & Verhagen, E. Optical circulation in a multimode optomechanical resonator. Nat. Commun. **9**, 1798 (2018).

[S20] Mathew, J. P., Pino, J. d. & Verhagen, E. Synthetic gauge fields for phonon transport in a nano-optomechanical system. Nat. Nanotechnol. **15**, 198 (2020).

[S21] Chen, Y. *et al*. Synthetic Gauge Fields in a Single Optomechanical Resonator. Phys. Rev. Lett. **126**, 123603 (2021).

[S22] Jing, H., Özdemir, Ş. K., Lü, X.-Y., Zhang, J., Yang, L. & Nori, F. $\mathcal{PT}$-Symmetric Phonon Laser. Phys. Rev. Lett. **113**, 053604 (2014).

[S23] Kato, T. *Perturbation Theory for Linear Operators*. (Springer, 2013).

[S24] Heiss, W. D. Phases of wave functions and level repulsion. Eur. Phys. J. D **7**, 1 (1999).

[S25] El-Ganainy, R., Makris, K. G., Khajavikhan, M., Musslimani, Z. H., Rotter, S. & Christodoulides, D. N. Non-Hermitian physics and $\mathcal{PT}$ symmetry. Nat. Phys. **14**, 11 (2018).

[S26] Parto, M., Liu, Y. G. N., Bahari, B., Khajavikhan, M. & Christodoulides, D. N. Non-Hermitian and topological photonics: optics at an exceptional point. Nanophotonics **10**, 403 (2021).

[S27] Makris, K. G., El-Ganainy, R., Christodoulides, D. N. & Musslimani, Z. H. Beam dynamics in $\mathcal{PT}$ symmetric optical lattices. Phys. Rev. Lett. **100**, 103904 (2008).

[S28] Klaiman, S., Günther, U. & Moiseyev, N. Visualization of branch points in $\mathcal{PT}$-symmetric waveguides. Phys. Rev. Lett. **101**, 080402 (2008).

[S29] Zheng, M. C., Christodoulides, D. N., Fleischmann, R. & Kottos, T. $\mathcal{PT}$ optical lattices and universality in beam dynamics, Phys. Rev. A **82**, 010103 (2010).

[S30] Bender, C. M. & Boettcher, S. Real Spectra in NonHermitian Hamiltonians Having $\mathcal{PT}$ Symmetry. Phys. Rev. Lett. **80**, 5243 (1998).

[S31] Bender, C. M. Making sense of non-Hermitian Hamiltonians. Rep. Prog. Phys. **70**, 947 (2007).

[S32] Khanikaev, A. B.*et al*. Photonic topological insulators. Nat. Mater. **12**, 233 (2013).

[S33] Özdemir, Ş. K., Rotter, S., Nori, F. & Yang, L. Parity-time symmetry and exceptional points in photonics. Nat. Mater. **18**, 783 (2019).

[S34] Pile, F. P. D. Gaining with loss. Nat. Photonics **11**, 742 (2017).

[S35] Chen, C., Jin, L. & Liu, R.-B. Sensitivity of parameter estimation near the exceptional point of a non-Hermitian system. New J. Phys. **21**, 083002 (2019).

[S36] Pickup, L., Sigurdsson, H., Ruostekoski, J. & Lagoudakis, P. G. Synthetic band-structure engineering in polariton crystals with non-hermitian topological phases. Nat. Commun. **11**, 4431 (2020).

[S37] Bergholtz, E. J., Budich, J. C. & Kunst, F. K. Exceptional topology of non-Hermitian systems. Rev. Mod. Phys. **93**, 015005 (2021).

[S38] Nair, J. M. P., Mukhopadhyay, D. & Agarwal, G. S. Enhanced Sensing of Weak Anharmonicities through Coherences in Dissipatively Coupled Anti-PT Symmetric Systems. Phys. Rev. Lett. **126**, 180401 (2021).

[S39] Pino, J. d., Slim, J. J. & Verhagen, E. Non-Hermitian chiral phononics through optomechanically induced squeezing. Nature **606**, 82 (2022).

[S40] Uzdin, R., Mailybaev, A. & Moiseyev, N. On the observability and asymmetry of adiabatic state flips generated by exceptional points. J. Phys. A **44**, 435302 (2011).

[S41] Graefe, E.-M., Mailybaev, A. A. & Moiseyev, N. Breakdown of adiabatic transfer of light in waveguides in the presence of absorption.

Phys. Rev. A **88**, 033842 (2013).
[S42] Choi, Y., Hahn, C., Yoon, J. W., Song, S. H. & Berini, P. Extremely broadband, on-chip optical nonreciprocity enabled by mimicking nonlinear anti-adiabatic quantum jumps near exceptional points. Nat. Commun. **8**, 14154 (2017).
[S43] Yoon, J. W. *et al.* Time-asymmetric loop around an exceptional point over the full optical communications band. Nature **562**, 86 (2018).
[S44] Ren, H. *et al.* Topological phonon transport in an optomechanical system. Nat. Comm. **13**, 3476 (2022).
[S45] Abbasi, M., Chen, W., Naghiloo, M., Joglekar, Y. N. & Murch, K. W. Topological Quantum State Control through Exceptional-Point Proximity. Phys. Rev. Lett. **128**, 160401 (2022).
[S46] Hassan, A. U., Zhen, B., Soljačić, M., Khajavikhan, M. & Christodoulides, D. N. Dynamically encircling exceptional points: exact evolution and polarization state conversion. Phys. Rev. Lett. **118**, 093002 (2017).
[S47] Wang, H., Assawaworrarit, S. & Fan, S. Dynamics for encircling an exceptional point in a nonlinear non-Hermitian system. Opt. Lett. **44**, 638 (2019).
[S48] Hassan, A. U. *et al.* Chiral state conversion without encircling an exceptional point. Phys. Rev. A **96**, 052129 (2017).
[S49] Zhong, Q., Khajavikhan, M., Christodoulides, D. N. & El-Ganainy, R. Winding around non-Hermitian singularities. Nat. Commun. **9**, 4808 (2018).
[S50] Feilhauer, J. *et al.* Encircling exceptional points as a non-Hermitian extension of rapid adiabatic passage. Phys. Rev. A **102**, 040201(R) (2020).
[S51] Nasari, H. *et al.* Observation of chiral state transfer without encircling an exceptional point, Nature **605**, 256 (2022).
[S52] Arkhipov, I. I., Miranowicz, A., Minganti, F., Özdemir, Ş. K. & Nori, F. Dynamically crossing diabolic points while encircling exceptional curves: A programmable symmetric-asymmetric multimode switch. Nat. Commun. **14**, 2076 (2023).
[S53] Chegnizadeh, M., Scigliuzzo, M., Youssefi, A., Kono, S., Guzovskii, E. & Kippenberg, T. J. Quantum collective motion of macroscopic mechanical oscillators. Science **386**, 1383 (2024).
[S54] Wilson-Rae, I., Nooshi, N., Zwerger, W. & Kippenberg, T. J. Theory of Ground State Cooling of a Mechanical Oscillator Using Dynamical Backaction. Phys. Rev. Lett. **99**, 093901 (2007).
[S55] Marquardt, F., Chen, J. P., Clerk, A. A. & Girvin, S. M. Quantum Theory of Cavity-Assisted Sideband Cooling of Mechanical Motion. Phys. Rev. Lett. **99**, 093902 (2007).
[S56] Chan, J. *et al.* Laser cooling of a nanomechanical oscillator into its quantum ground state. Nature **478**, 89 (2011).
[S57] Teufel, J. D. *et al.* Sideband cooling of micromechanical motion to the quantum ground state. Nature **475**, 359 (2011).